



Since January 2020 Elsevier has created a COVID-19 resource centre with free information in English and Mandarin on the novel coronavirus COVID-19. The COVID-19 resource centre is hosted on Elsevier Connect, the company's public news and information website.

Elsevier hereby grants permission to make all its COVID-19-related research that is available on the COVID-19 resource centre - including this research content - immediately available in PubMed Central and other publicly funded repositories, such as the WHO COVID database with rights for unrestricted research re-use and analyses in any form or by any means with acknowledgement of the original source. These permissions are granted for free by Elsevier for as long as the COVID-19 resource centre remains active.



## Article

# Vaccine-elicited murine antibody WS6 neutralizes diverse beta-coronaviruses by recognizing a helical stem supersite of vulnerability

Wei Shi,<sup>1,4</sup> Lingshu Wang,<sup>1,4</sup> Tongqing Zhou,<sup>1,4</sup> Mallika Sastry,<sup>1</sup> Eun Sung Yang,<sup>1</sup> Yi Zhang,<sup>1</sup> Man Chen,<sup>1</sup> Xuejun Chen,<sup>1</sup> Misook Choe,<sup>1</sup> Adrian Creanga,<sup>1</sup> Kwan Leung,<sup>1</sup> Adam S. Olia,<sup>1</sup> Amarendra Pegu,<sup>1</sup> Reda Rawi,<sup>1</sup> Arne Schön,<sup>2</sup> Chen-Hsiang Shen,<sup>1</sup> Erik-Stephane D. Stancovski,<sup>1</sup> Chloe Adrienna Talana,<sup>1</sup> I-Ting Teng,<sup>1</sup> Shuishu Wang,<sup>1</sup> Kizzmekia S. Corbett,<sup>1</sup> Yaroslav Tsybovsky,<sup>3</sup> John R. Mascola,<sup>1,\*</sup> and Peter D. Kwong<sup>1,5,\*</sup>

<sup>1</sup>Vaccine Research Center, National Institute of Allergy and Infectious Diseases, National Institutes of Health, Bethesda, MD 20892, USA

<sup>2</sup>Department of Biology, Johns Hopkins University, Baltimore, MD 21218, USA

<sup>3</sup>Electron Microscopy Laboratory, Cancer Research Technology Program, Leidos Biomedical Research, Inc., Frederick National Laboratory for Cancer Research, Frederick, MD 21702, USA

<sup>4</sup>These authors contributed equally

<sup>5</sup>Lead contact

\*Correspondence: [jmascola@icloud.com](mailto:jmascola@icloud.com) (J.R.M.), [pdkwong@nih.gov](mailto:pdkwong@nih.gov) (P.D.K.)

<https://doi.org/10.1016/j.str.2022.06.004>

## SUMMARY

Immunization with severe acute respiratory syndrome coronavirus 2 (SARS-CoV-2) spike elicits diverse antibodies, but it is unclear if any of the antibodies can neutralize broadly against other beta-coronaviruses. Here, we report antibody WS6 from a mouse immunized with mRNA encoding the SARS-CoV-2 spike. WS6 bound diverse beta-coronavirus spikes and neutralized SARS-CoV-2 variants, SARS-CoV, and related sarbecoviruses. Epitope mapping revealed WS6 to target a region in the S2 subunit, which was conserved among SARS-CoV-2, Middle East respiratory syndrome (MERS)-CoV, and hCoV-OC43. The crystal structure at 2 Å resolution of WS6 revealed recognition to center on a conserved S2 helix, which was occluded in both pre- and post-fusion spike conformations. Structural and neutralization analyses indicated WS6 to neutralize by inhibiting fusion and post-viral attachment. Comparison of WS6 with other recently identified antibodies that broadly neutralize beta-coronaviruses indicated a stem-helical supersite—centered on hydrophobic residues Phe1148, Leu1152, Tyr1155, and Phe1156—to be a promising target for vaccine design.

## INTRODUCTION

The coronavirus disease 2019 (COVID-19) pandemic, resulting from the zoonotic infection of severe acute respiratory syndrome coronavirus 2 (SARS-CoV-2), has lasted more than 2 years with more than 500 million cases and over 6 million deaths (<https://www.who.int/publications/m/item/weekly-epidemiological-update-on-covid-19>). Continuously evolving variants are making current licensed vaccines less effective (Araf et al., 2022; Edara et al., 2021; Garcia-Beltran et al., 2022; Liu et al., 2021; Pajon et al., 2022). Vaccines capable of neutralizing all SARS-CoV-2 variants for the foreseeable future are of high interest. Antibodies with broad neutralizing capacity are also of interest: if ultrapotent, they might be useful as therapeutic antibodies, but even if they are only of moderate potency, their epitopes are useful as vaccine templates (Kong et al., 2016).

Virtually all SARS-CoV-2 neutralizing antibodies are directed against the trimeric ectodomain of the spike glycoprotein, which comprises two subunits, S1 and S2. Neutralizing antibodies isolated from COVID-19 convalescent donors or from vaccinees after

spike immunization are directed primarily against the N-terminal domain (NTD) or receptor-binding domain (RBD) on the S1 subunit of the trimeric viral surface spike glycoprotein (spike) (Barnes et al., 2020; Brouwer et al., 2020; Cao et al., 2020; Cerutti et al., 2021; Ju et al., 2020; Liu et al., 2020; McCallum et al., 2021; Robbiani et al., 2020; Rogers et al., 2020; Seydoux et al., 2020; Suryadevara et al., 2021; Zost et al., 2020). Several recently emerged SARS-CoV-2 variants, such as Delta and Omicron, evade these antibodies by mutations that reduce or knock out antibody binding but maintain or even enhance infectivity (Garcia-Beltran et al., 2022; Liu et al., 2021; Sievers et al., 2022; Syed et al., 2022). Antibodies against most other regions on the spike are generally poorly neutralizing to non-neutralizing; several antibodies, however, such as antibodies 28D9 (Wang et al., 2021a) and S2P6 (Pinto et al., 2021) have been reported to neutralize diverse strains of beta-coronaviruses through recognition of a stem-helix supersite of vulnerability in the S2 subunit (Hsieh et al., 2021; Li et al., 2022; Sauer et al., 2021; Zhou et al., 2021).

To investigate the breadth of neutralizing antibodies obtained from mice vaccinated by mRNA encoding the SARS-CoV-2



spike, we assessed monoclonal antibodies for the location of their epitopes, the breadth of their binding to diverse spikes, and their neutralization capacities. We found one antibody, WS6, with broad binding capacity and moderate neutralization potency, and we determined its crystal structure in complex with its epitope, the step in the entry pathway where it neutralized, and how its recognition compared with other recently identified antibodies with overlapping epitopes. The results reveal a highly promising vaccine target in the S2 subunit—comprising a hydrophobic cluster spanning three helical turns, with acidic residues framing the central turn—and add WS6 to the panel of antibodies by which to guide its vaccine development.

## RESULTS

### Identification and characterization of SARS-CoV-2 spike-specific antibodies from immunized mice

To obtain antibodies specific for SARS-CoV-2 spike glycoprotein, we immunized mice with mRNA coding for SARS-CoV-2 spike (Figure 1A). To generate hybridomas, we boosted with soluble spike protein and, after 3 days, generated hybridomas by fusing splenocyte B cells with Sp2/0 cells from the mouse with the highest plasma neutralization titers to SARS-CoV-2. Eleven monoclonal antibodies, named WS1 to WS11, bound SARS-CoV-2 S-dTM (spike residues 1–1,206) by ELISA (Figure 1B). Nine of these bound the S1 subunit, either S1-short1 (spike residues 1–670) or S1R (residues 1–537). Six of them, WS1, WS2, WS3, WS7, WS8, and WS10, bound NTD, and three of them, WS4, WS9, and WS11, bound RBD. Antibodies WS5 and WS6, however, did not bind NTD, RBD, or S1, and their binding epitopes were presumably on the S2 subunit of the spike.

To provide insight into the breadth of binding, we assessed recognition of WS1–11 on a panel of prefusion-stabilized diverse beta-coronavirus spikes (S2Ps) (Wrapp et al., 2020). Detectable binding was observed against SARS-CoV-2, SARS-CoV, Middle East respiratory syndrome (MERS)-CoV, and hCoV-HKU1 for five antibodies (Figure 1C). For antibodies WS3, WS4, and WS7, binding was more than 1,000-times weaker against the divergent strain versus that of the immunogen. However, for antibodies WS5 and WS6, binding was only about 10-fold reduced versus SARS-CoV-2. Neutralization assessments revealed that WS5 neutralized neither SARS-CoV-2 nor SARS-CoV, whereas WS6 could neutralize both (Figure 1D). WS6 was further studied for its epitope and neutralization activities.

### WS6 recognizes diverse beta-coronaviruses spikes and neutralizes SARS-CoV-2 and variants, SARS-CoV, and related viruses from bat, pangolin, and other animals

To assess fully the broad reactivity of WS6, we performed ELISAs against S2Ps from an even more divergent panel of coronaviruses, including RaTG13, WIV1, SHC014, hCoV-OC43, and hCoV-229E (Figure 2A). Remarkably, WS6 was able to bind all beta-coronaviruses tested, though not to the alpha-coronavirus hCoV-229E (Figure S1). The binding affinities of WS6 to S2Ps, measured by surface plasmon resonance (SPR), showed nanomolar or lower dissociation constants ( $K_D$ s) (Figure 2B). Isothermal titration calorimetry (ITC) analysis of WS6 binding to SARS-CoV-2 S2P revealed a  $K_D$  of 2.6 nM (Figure 2C), confirming the low nanomolar  $K_D$ s obtained by SPR. To determine if

WS6 could bind spike proteins on cell surface, we expressed spikes of SARS-CoV-2, SARS-CoV, MERS-CoV, hCoV-HKU1, and hCoV-OC43 on the surface of Expi-293 cells and analyzed WS6 binding by flow cytometry. We found that WS6 bound well to the cell surface expressing the beta-coronavirus spikes (Figures 2D and S2).

To determine if the broad recognition of WS6 for spikes translated into broad neutralization of beta-coronaviruses, we assessed its neutralization activities by pseudovirus neutralization assays (Naldini et al., 1996; Wang et al., 2021b). WS6 neutralized all tested variants of SARS-CoV-2 including Omicron (B.1.1.529), with half-maximal inhibitory concentrations ( $IC_{50}$ s) 2.46–26.52  $\mu$ g/mL (Figures 2E and S3; Table S1). WS6 could also neutralize beta-coronaviruses related to SARS-CoV-2 (such as RaTG13, Pangolin\_GD, and Pangolin\_GX), SARS-CoV, and related viruses Frankfurt1, Civet007-2004, WIV1, and SHC014 with  $IC_{50}$ s 0.11–4.91  $\mu$ g/mL (Figures 2E and S3; Table S1). WS6 also neutralized related beta-coronaviruses, such as RaTG13, Pangolin-GX, Civet007-2004, and SHC014, with submicromolar  $IC_{50}$ s, better than against SARS-CoV-2 despite being elicited by immunizations with SARS-CoV-2 spike. The only tested beta-coronavirus strain WS6 failed to neutralize was MERS-CoV, consistent with its lower ELISA binding to this strain (Table S1).

Several S2-directed antibodies have recently been reported, including the antibody S2P6 (Pinto et al., 2021), which broadly neutralizes beta-coronaviruses including MERS-CoV. We compared WS6 and S2P6 for neutralization against diverse SARS-CoV-2 variants and diverse coronaviruses (Figure S3). Despite its high breadth, S2P6 was unable to neutralize the Omicron variant of SARS-CoV-2, whereas WS6 did neutralize Omicron. WS6 neutralized all tested strains more potently than S2P6, except for MERS-CoV, against which WS6 was non-neutralizing. The two recently reported murine antibodies, B6 and immunoglobulin G22 (IgG22), utilize the same heavy-chain origin gene (VH1-19), and both generated after immunization with spikes from SARS-CoV-2 and MERS-CoV (Hsieh et al., 2021; Pinto et al., 2021). By contrast, WS6 used a different V gene and was generated by immunization with the SARS-CoV-2 spike only—thereby revealing a new mode of murine S2-helix recognition and showing that MERS-CoV spike immunization was not required to elicit these antibodies.

### WS6 epitope mapping

We attempted to map the epitope of WS6 by visualizing its recognition of the spike ectodomain by negative-stain electron microscopy (EM). Two-dimensional (2D) classification of antigen-binding fragment (Fab) of WS6 in complex with the S2P spike (WA-1 strain) showed generally unbound spikes, with only 4% of the images yielding a trimer with Fabs binding in the membrane-proximal S2 stem (Figure 3A). We also analyzed Fab WS6 in complex with spike S2 subunit; 2D classification indicated WS6 to bind S2, though most of S2 appeared to be disordered and not in a typical pre- or post-fusion conformation (Figure 3B).

To further map the epitope, we performed peptide-array-based epitope mapping and identified a 17-residue peptide, PELDSFKEELDKYFKNH (SARS-CoV-2 spike residues 1,143–1,159) to bind WS6 (Figure 3C), suggesting the WS6 epitope to

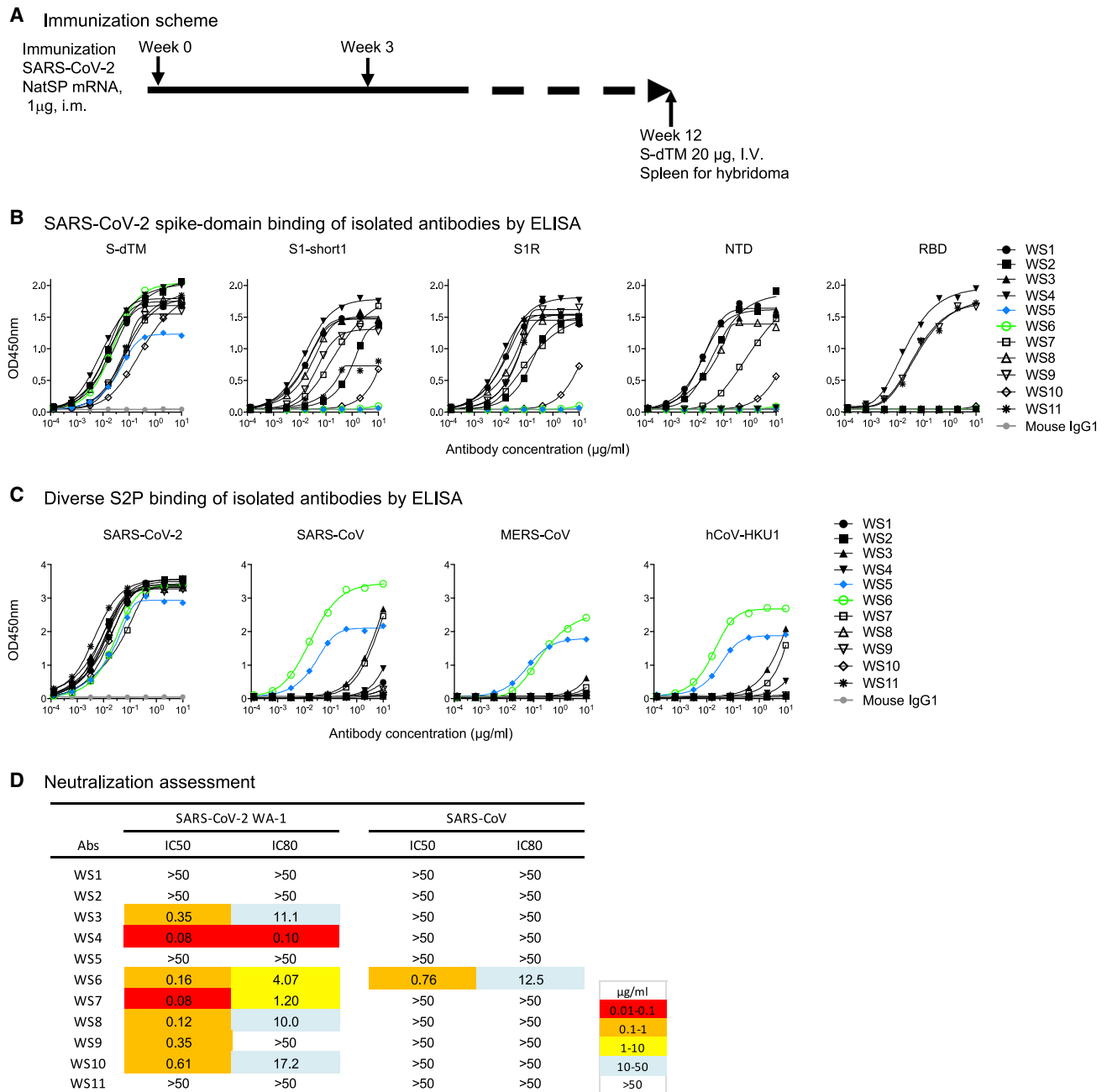


**Figure 1. Spike-mRNA-immunized mice elicit antibodies against diverse regions of spike, several of which bound diverse beta-coronavirus spikes and one of which, WS6, neutralized them**

(A) Immunization scheme. NatSP is the full transmembrane-containing native sequence of spike WA-1 strain; S-dTM is the soluble spike protein residues 1–1,206 of wild-type WA-1 strain.

(B) Binding of isolated antibodies by ELISA to subdomains of the SARS-CoV-2 spike. Purified monoclonal antibodies from hybridoma supernatants were analyzed for binding to SARS-CoV-2 S-dTM, S1 (S1-short and S1R), RBD, and NTD by ELISA.

(C) Binding of isolated antibodies assessed by ELISA to diverse beta-coronavirus pre-fusion-stabilized spikes (S2Ps).

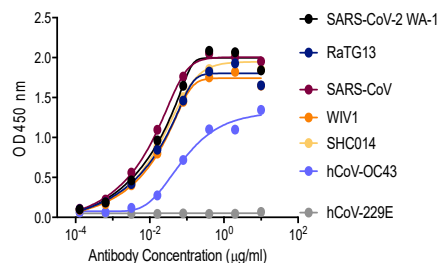
(D) Neutralization assessment of hybridoma antibodies against SARS-CoV-2 WA-1 and SARS-CoV pseudoviruses on 293T-ACE2 cells.

See also Figure S1.

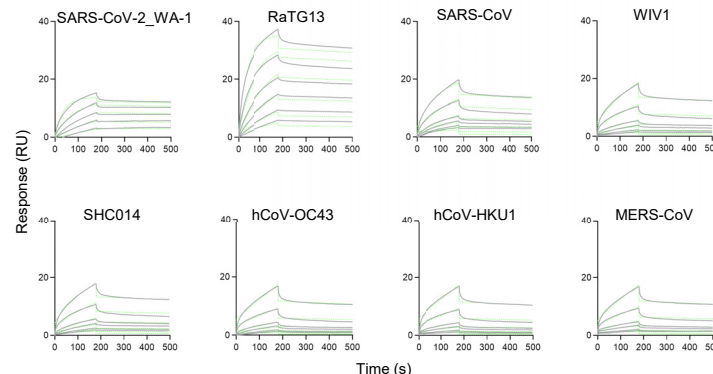
be at the S2 stem-helix region of the spike near the viral membrane, consistent with our negative-stain EM observation. This peptide is conserved among SARS-CoV, SARS-CoV-2, and RaTG13 and is mostly conserved among diverse beta-coronavirus

(Figure S4A). A similar peptide (residues 1,148–1,159) has been identified as a highly immunogenic linear epitope from sera of 1,051 patients with COVID-19 (Li et al., 2021). We used ITC to measure the affinity between WS6 and three peptides, two from

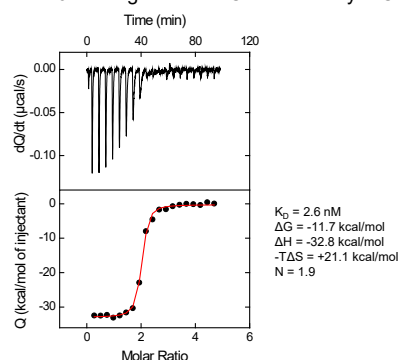
**A** WS6 binding to CoV spike proteins by ELISA



**B** WS6 Fab binding to diverse CoV spike S2P by Surface Plasmon Resonance

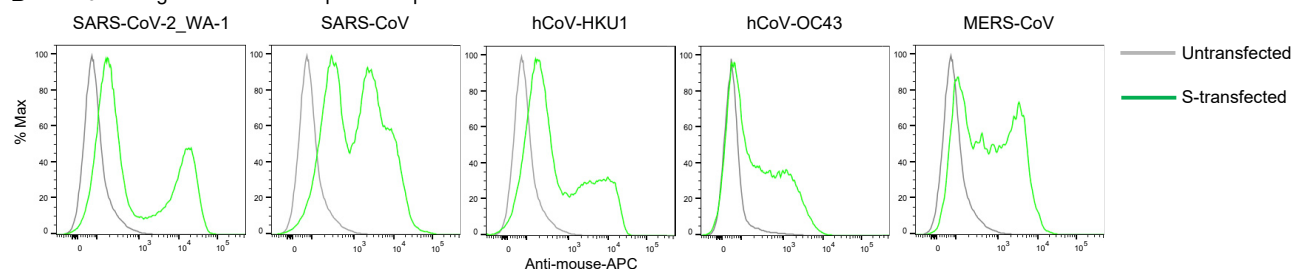


**C** WS6 binding to SARS-CoV-2 S2P by ITC



Spike Protein	$k_a$ (1/Ms)	$k_d$ (1/s)	$K_D \pm SE$ (nM)
SARS-CoV-2 WA-1	$2.59 \times 10^5$	$1.05 \times 10^{-4}$	$0.41 \pm 0.008$
RaTG13	$1.22 \times 10^5$	$1.56 \times 10^{-4}$	$1.27 \pm 0.03$
SARS-CoV	$5.22 \times 10^4$	$3.15 \times 10^{-4}$	$6.03 \pm 0.16$
WIV1	$1.76 \times 10^4$	$2.74 \times 10^{-4}$	$15.54 \pm 0.41$
SHC014	$2.78 \times 10^4$	$2.28 \times 10^{-4}$	$8.22 \pm 0.24$
hCoV-OC43	$5.14 \times 10^2$	$3.08 \times 10^{-4}$	$596 \pm 33.80$
hCoV-HKU1	$4.25 \times 10^2$	$3.38 \times 10^{-4}$	$796 \pm 26.50$
MERS-CoV	$6.46 \times 10^3$	$3.26 \times 10^{-4}$	$50.47 \pm 2.86$

**D** WS6 binding to cell surface expressed spikes



**E** WS6 neutralization of pseudoviruses

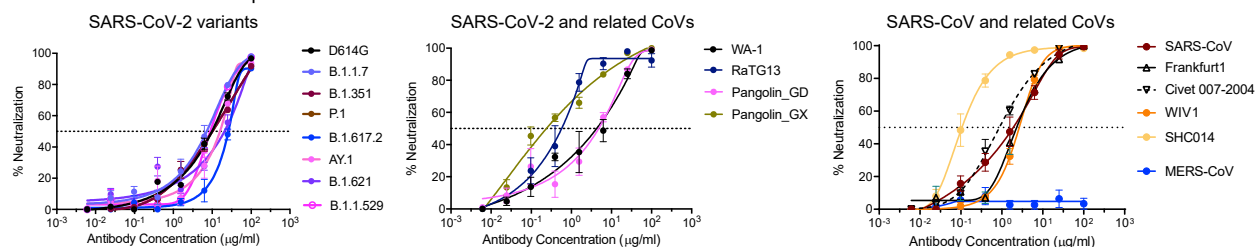
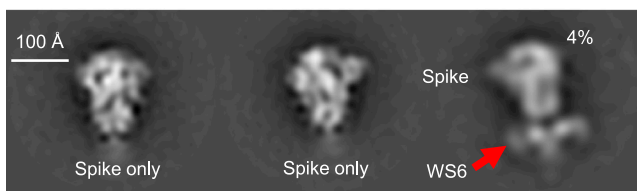


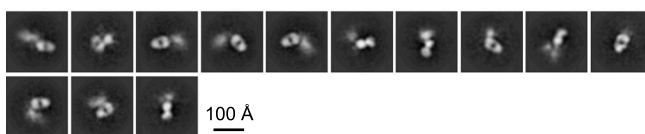
**Figure 2. Antibody WS6 binds and neutralizes diverse beta-coronaviruses**

(A) ELISA binding analysis of WS6 to pre-fusion-stabilized soluble spikes of various coronaviruses. (B) Surface plasmon resonance (SPR) binding curves of WS6 Fab with various beta-coronaviruses. (C) Thermodynamics of WS6 binding to SARS-CoV-2 S2P. WS6 IgG was titrated into S2P in the cell at 25°C. (D) WS6 binds cell-surface-expressed spike proteins from SARS-CoV-2, SARS-CoV, hCoV-HKU1, hCoV-OC43, and MERS-CoV. (E) WS6 neutralizes SARS-CoV-2 variants, SARS-CoV, and related animal coronaviruses. All neutralization activity was measured using spike-pseudotyped lentivirus on 293 flpIn-TMPRSS2-ACE2 cells except for MERS-CoV, which was tested on Huh7.5 cells. Assays were performed in triplicate, and representative neutralization curves from two to three technical replicates are shown. Data are represented as mean percentages of neutralization with SEM calculated from the triplicate wells. (Left) WS6 neutralizes SARS-CoV-2 variants, D614G, B.1.1.7 (Alpha), B.1.351 (Beta), P.1 (Gamma), B.1.617.2 (Delta), AY.1 (Delta+), B.1.621 (Mu), and B.1.1.529 (Omicron). (Middle) WS6 neutralizes SARS-CoV-2 and related coronaviruses, SARS-CoV-2 WA-1, RaTG13, Pangolin\_GD, and Pangolin\_GX. (Right) WS6 neutralizes SARS-CoV and related coronaviruses, SARS-CoV, Frankfurt1, Civet 007-2004, WIV1, and SHC014 but not MERS-CoV. See also [Figures S1–S3](#) and [Table S1](#).

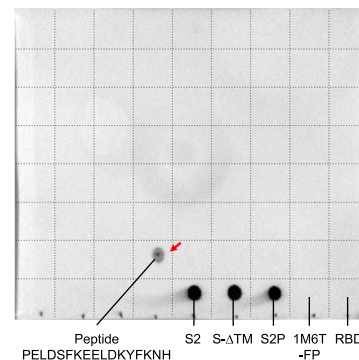
**A** Negative stain EM of WS6 in complex with SARS-CoV-2 spike



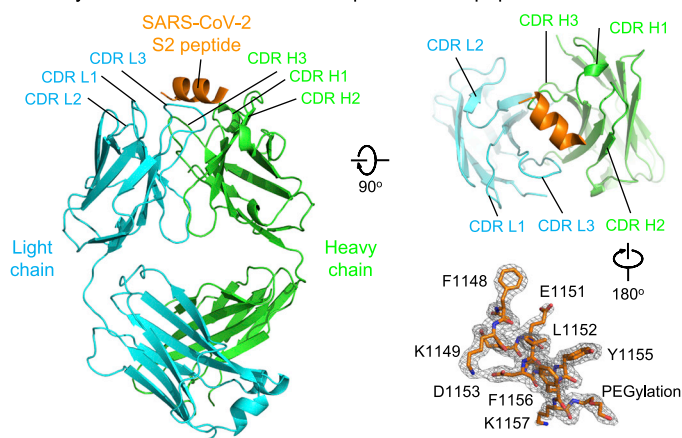
**B** Negative stain EM of WS6 in complex with SARS-CoV-2 spike S2



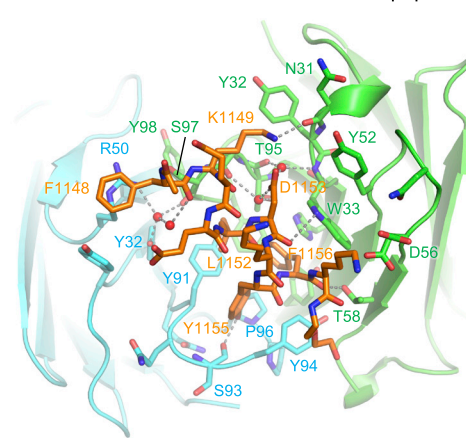
**C** Mapping the epitope with a SARS-CoV spike peptide array



**D** Crystal structure of WS6 in complex with S2 peptide at 2.0 Å resolution



**E** Interactions between WS6 and S2 peptide



**F** WS6 sequence and paratope

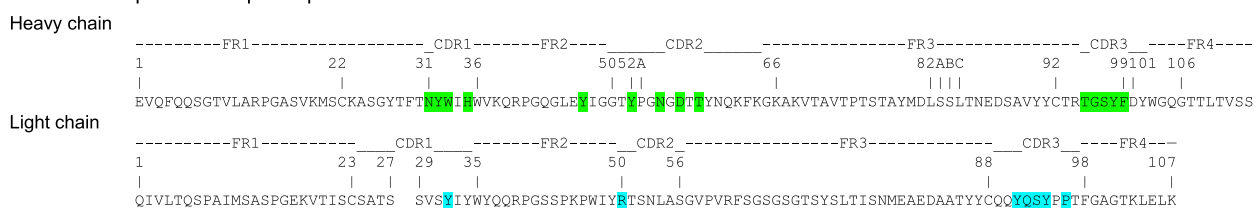


**Figure 3. Epitope mapping and crystal structure of antibody WS6 in complex with S2 peptide**

(A) Negative-stain EM of SARS-CoV-2 spike in complex with WS6. Only a small fraction was observed with WS6 bound at the stem region. Scale bar represents 100 Å.

(B) Negative-stain EM of SARS-CoV-2 spike S2 in complex with WS6. Scale bar represents 100 Å.

(C) Epitope mapping by dot-blot assay with a SARS-CoV spike peptide array (BEI, NR-52418). WS6 bound to peptide #154 P<sub>1125</sub>ELDSFKEELDKYFKNH<sub>1141</sub> (corresponding to SARS-CoV-2 residues 1,143–1,159) (red arrow), SARS-CoV-2 spike (S-ΔTM and S2P) and its S2 domain, but not scaffold-fusion peptide (1M6T-FP) nor RBD. A dash line grid has been added on top of the blot to aid display.

(D) Crystal structure of WS6 in complex with SARS-CoV-2 S2 peptide at 2.0 Å resolution. The antibody and SARS-CoV-2 peptide are shown in cartoon representation. WS6 heavy chain, light chain, and S2 peptide are colored green, cyan, and orange, respectively. Two 90°-flipped views are shown (left, top right). 2Fo-Fc electron density map of the S2 peptide is shown at 1.2 σ, with the antibody interacting residues facing the reader (right, bottom) in a 180°-flipped view from panel above. Molecular structure figures were prepared with PyMOL.

(E) Detailed interactions between WS6 and S2 peptide. The S2 peptide and WS6 are shown in sticks and representation, with other regions of WS6 shown in cartoon representation. Hydrogen bonds are indicated with gray dashed lines. Waters that mediating hydrogen bonds are shown as red spheres.

(F) Sequence and paratope of WS6. WS6 residues are numbered according to Kabat nomenclature. Heavy and light chain paratope residues are highlighted in green and cyan, respectively.

See also [Figure S5](#) and [Table S2](#).

**Table 1. Crystallographic data and refinement statistics**

Data collection	
Wavelength (Å)	1.0000
Resolution range (Å)	40.23–2.02 (2.092–2.02)
Space group	C 1 2 1
Unit cell (a, b, c, $\alpha$ , $\beta$ , $\gamma$ )	155.1, 64.5, 138.0, 90.0, 117.3, 90.0
Total reflections	262,622
Unique reflections <sup>a</sup>	75,855 (6,642)
Multiplicity	3.5 (2.9)
Completeness (%)	94.81 (81.69)
I/ $\sigma$ I	10.5 (1.1)
R-merge	0.101 (0.943)
R-pim	0.083 (0.513)
CC <sub>1/2</sub>	0.995 (0.765)
Refinement	
Reflections used in refinement	75,540 (6,475)
Reflections used for R-free	1,989 (170)
R-work	0.1718 (0.2427)
R-free	0.2133 (0.2848)
Number of non-hydrogen atoms	7,587
Macromolecules	6,696
Ligands	176
Solvent	735
Protein residues	871
RMS (bonds, Å)	0.008
RMS (angles, °)	0.91
Ramachandran favored (%)	97.78
Ramachandran allowed (%)	2.22
Ramachandran outliers (%)	0.00
Rotamer outliers (%)	0.92
Clashscore	4.58
Average B factor (Å <sup>2</sup> )	32.90
Macromolecules	31.84
Ligands	49.90
Solvent	38.92

<sup>a</sup>Statistics for the highest-resolution shell are shown in parentheses.

SARS-CoV-2 (of 10 or 25 residues) and one from MERS-CoV, and we observed  $K_D$ s of 22 and 0.25 nM for the short and long SARS-CoV-2 peptides, respectively, and a  $K_D$  of 390 nM for the MERS-CoV peptide (Figure S5).

### Crystal structure of WS6 in complex with a conserved S2 peptide

To elucidate the mechanism for the broad reactivity of WS6, we determined a crystal structure at 2 Å of Fab WS6 in complex with peptide Ace-F<sub>1148</sub>KEELDKYFK<sub>1157</sub>-PEG12-Lys-Biotin (residue numbers were based on the SARS-CoV-2 spike sequence) (Figures 3D; Table 1). The peptide contained a 10-residue segment conserved among beta-coronaviruses (Figure S4A) and was acetylated at the N terminus and biotin-pegylated at the C terminus. Well-defined electron density was observed for

the entire WS6 Fab and for the entire peptide, including the acetyl group at the N terminus and part of the polyethylene glycol at the C terminus (Figure 3D). Peptide-binding interactions involved both heavy and light chains, with the heavy chain contributing  $\sim 360$ -Å<sup>2</sup> buried surface area (BSA) and the light chain contributing  $\sim 230$  Å<sup>2</sup> (Table S2), analyzed with PDBePISA (Krissinel and Henrick, 2007). The BSA of the peptide was slightly larger at  $\sim 675$  Å<sup>2</sup>, not counting the BSA of the visible PEG fragment ( $\sim 100$  Å<sup>2</sup> total). This binding interface is smaller than a typical antibody-binding epitope, indicating the full WS6 epitope to likely involve additional residues.

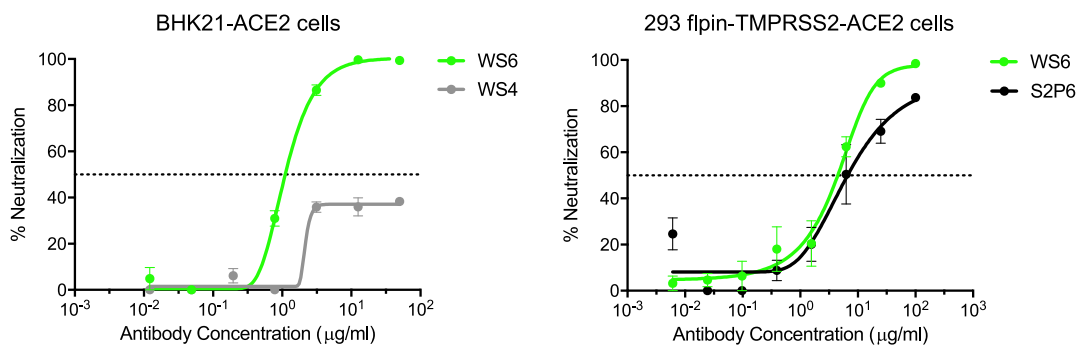
All complementarity-determining regions (CDRs) of both heavy and light chains were involved in binding, creating a groove that cradled the epitope (Figure 3D). In the WS6-bound crystal structure, the S2 epitope formed a three-turn  $\alpha$  helix; examination of its binding mode revealed binding for a longer helix with extensions on both termini without any major clashes. Most of the residues of the peptide were involved in binding, except for Glu1150 and Lys1154, which were on the opposite side of the helix facing WS6 (Figure 3E). Aromatic or hydrophobic residues, Phe1148, Leu1152, Tyr1155, and Phe1156, were on the side of the helix facing WS6. Phe1148 had aromatic interactions with Arg50<sub>L</sub> and Tyr91<sub>L</sub> of the WS6 light chain and hydrophobic interactions with Ser97<sub>H</sub> of the heavy chain. The Tyr1155 side chain stuck into a cavity formed by CDR L3 from Tyr91<sub>L</sub> to Pro96<sub>L</sub> and had aromatic or hydrophobic interactions with side chains of Tyr91<sub>L</sub>, Tyr94<sub>L</sub>, and Pro96<sub>L</sub> and the peptide backbone. Leu1152 and Phe1156 side chains bound in a pocket between heavy and light chains and interacted with side chains of Tyr91<sub>L</sub>, Pro96<sub>L</sub>, Phe99<sub>H</sub>, Thr95<sub>H</sub>, Trp33<sub>H</sub>, His35<sub>H</sub>, and Tyr47<sub>H</sub> (Figures 3E and 3F; Table S2).

### WS6 neutralizes by inhibition of fusion steps post-viral attachment

To elucidate the mechanism by which WS6 neutralizes beta-coronaviruses, we incubated BHK21-ACE2 cells with SARS-CoV-2 spike-pseudotyped lentivirus on ice to allow virus to attach to ACE2. After thorough washing, cells were incubated with WS6 or WS4 on ice for 1 h and at 37°C for 72 h. WS4, an RBD-directed neutralizing antibody, could neutralize not more than 40% of the virus, whereas WS6 had no problem neutralizing the ACE2 pre-attached virus (Figure 4A). We performed a similar experiment using 293 flpin-TMPRSS2-ACE2 cells for WS6 and S2P6 (Pinto et al., 2021), which also bind to the S2-stem helix, and found that both antibodies could neutralize ACE2 pre-attached virus. These results suggest that WS6 is likely to neutralize SARS-CoV-2 by engaging in steps post-viral attachment to ACE2.

As described above in the structural analysis, WS6 recognized the hydrophobic face of the stem helix with residues Phe1148, Leu1152, Tyr1155, and Phe1156 binding in the center of the paratope groove. In the pre-fusion structure of SARS-CoV-2 spike (PDB: 6XR8) (Cai et al., 2020; Ke et al., 2020), these hydrophobic side chains pack in the coiled-coil interface of the 3-helical bundle, indicating that the target site of WS6 and other similar antibodies on S2 stem is cryptic. Modeling of WS6 binding to the pre-fusion SARS-CoV-2 spike, based on the WS6-peptide complex, revealed substantial clashes (Figure 4B, left panel), indicating that WS6 binding would require unpacking or disassembly of the helical bundle. A previous study showed that binding of B6 disrupted/opened the prefusion MERS-CoV spike in

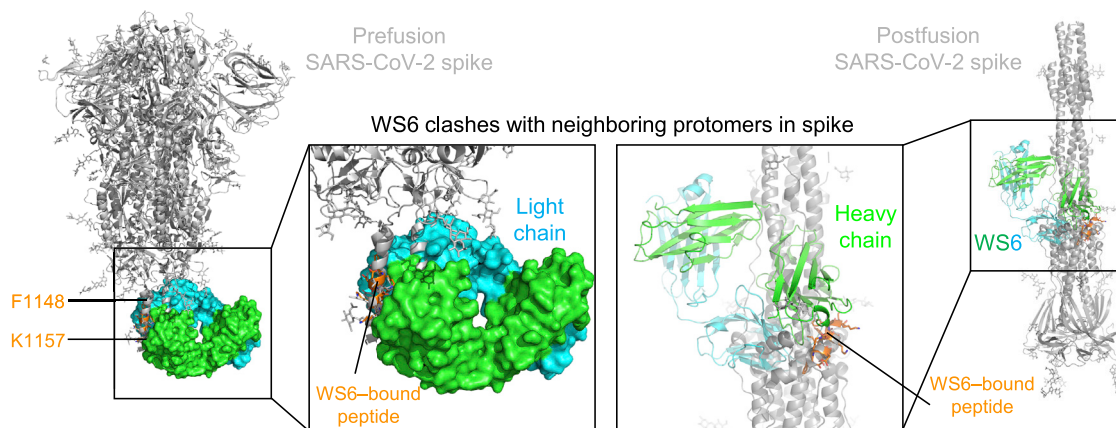
**A** WS6 inhibits post viral attachment



**B** WS6-binding is not compatible with the prefusion and postfusion conformation of the spike

WS6 superposed onto prefusion conformation

WS6 superposed onto the postfusion conformation



**C** Potential mechanism of neutralization

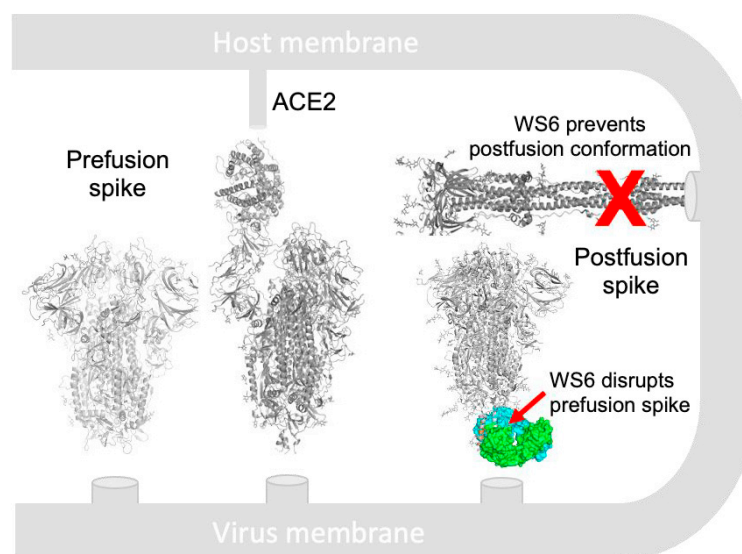


**Figure 4. WS6 neutralizes SARS-CoV-2 by inhibition of post-viral attachment**

(A) WS6 and S2P6 neutralization of SARS-CoV-2 by inhibition of post-viral attachment. Neutralization experiments were performed with BHK21-ACE2 (top) and 293 flpin-TMPRSS2-ACE2 (bottom) cells. WS4, an RBD antibody, was used as a negative control. Assays were performed in triplicate, and representative

(legend continued on next page)

the stem region to expose the epitope, while other regions of the spike remained in the pre-fusion state (Sauer et al., 2021). WS6 potentially utilizes the same mechanism to disrupt the helix bundle to achieve binding and prevent transition to the post-fusion state. Modeling also revealed that the post-fusion spike structure (PDB: 6XRA) (Cai et al., 2020) was incompatible with binding of WS6 to the hydrophobic side of the peptide helix, as revealed by the crystal structure, because these hydrophobic residues are involved in the packing of the small helix with the central coiled coil in the post-fusion structure (Figure 4B, right panel). Because the spike binding to the receptor and transitioning from the pre-fusion to the post-fusion conformation drive the membrane fusion process, WS6 maybe even more apt to bind during this conformational transition and inhibit the fusion process (Figure 4C).

### A helical stem supersite of vulnerability

Several broad beta-coronavirus neutralizing antibodies have been identified recently that target the S2 stem-helix region, including the aforementioned S2P6 (Pinto et al., 2021) as well as antibodies B6 (Sauer et al., 2021), IgG22 (Hsieh et al., 2021), CCP40.8 (Zhou et al., 2021), and CV3-25 (Hurlburt et al., 2021; Li et al., 2022). The superposition of their S2 helical epitopes indicated that these antibodies bound to the stem helix with varying orientations (Figure 5A) and targeted different sets of residues ranging from residue position 1,142 to 1,164 on S2 (Figures 5B and 5C). Epitope analysis indicated a common subset of residues, namely Phe1148, Lys1149, Glu1150, Leu1152, Asp1153, Tyr1155, and Phe1156, to interact with four of the six antibodies (Figure 5B, left). These residues, which spanned three helical turns on S2 with a central hydrophobic cluster sandwiched by hydrophilic residues Lys1149, Glu1150, and Asp1153, formed a supersite of vulnerability for antibody recognition (Figure 5B, middle and right). Sequence analysis indicated this S2 supersite to be highly conserved among beta-coronaviruses (Figure 5C), providing the basis for the broad neutralization by WS6 and other antibodies targeting this site. It is of note that change of WS6 epitope residues Lys1149 and Tyr1155 in SARS-CoV-2 to Gln and Phe in MERS-CoV S2 eliminates two hydrogen bonds between the S2 peptide and WS6, potentially weakens WS6 binding to MERS CoV spike, and leads to the loss of neutralization. Overall, these S2 stem-helix antibodies are likely to share a similar mechanism of neutralization. Before or even after spike binds to ACE2, the stem helix appears to adopt a conformation or conformations that expose this supersite, allowing for the stem-helix antibodies to bind and prevent spike conformations needed for fusion, thereby stalling the entry process. Importantly, these S2-helix-directed broad neutralizers have diverse origin genes, except for B6 and IgG22, which utilize the same VH gene and appear to be of the same antibody class. In addition, the antibodies have only low-to-moderate somatic hyper-

mutation, suggesting that diverse ontogenies are possible with little barrier to their development (Figure S4).

## DISCUSSION

Zoonotic infections from beta-coronaviruses have caused multiple pandemics and endemics in recent years, including SARS (Drosten et al., 2003; Ksiazek et al., 2003), MERS (Zaki et al., 2012), and the ongoing COVID-19 (Zhou et al., 2020a; Zhu et al., 2020). It seems likely that additional beta-coronavirus zoonotic pandemics will occur in the future. Broadly neutralizing antibodies or broad vaccines against a wide spectrum of beta-coronaviruses may be effective at preventing or ameliorating such pandemics—and could even be of use against the current COVID-19, if variants do succeed in escaping control by current vaccines. In this study, we isolated an S2-directed antibody, named WS6, from a mouse immunized with mRNA-encoded SARS-CoV-2 spike. WS6 could bind and neutralize all variants of SARS-CoV-2, including Delta and Omicron; it could also neutralize SARS-CoV, as well as bat, civet, and pangolin beta-coronaviruses related to SARS-CoV and SARS-CoV-2. The crystal structure of WS6, in complex with the S2 stem-helix epitope peptide, revealed the structural basis for broad recognition and, together with neutralization and binding analyses, suggested a potential mechanism by which WS6 neutralizes broad beta-coronaviruses.

Several other groups have recently reported S2-directed antibodies including antibodies S2P6 (Pinto et al., 2021), CC40.8 (Zhou et al., 2021), and CV3-25 (Li et al., 2022) from SARS-CoV-2-infected convalescent donors and B6 (Sauer et al., 2021) and IgG22 (Hsieh et al., 2021) from vaccinated mice. We compared WS6 with S2P6 for neutralization activities and found that S2P6 was unable to neutralize the Omicron variant of SARS-CoV-2, whereas WS6 was able to neutralize all tested SARS-CoV-2 variants including Omicron. WS6 also neutralized all tested beta-coronavirus strains more potently than S2P6, except for MERS-CoV. In terms of the murine broad beta-coronavirus neutralizing antibodies, WS6 used a different V gene from B6 and IgG22 and represented a new class of murine antibody with a new mode of S2-helix recognition. The fact that WS6 was generated by immunization with only SARS-CoV-2 spike indicates that immunization with SARS-CoV-2 spike alone is sufficient to elicit broad beta-coronavirus neutralizing antibodies.

It will be interesting to determine whether S2-helix peptide-based immunizations can focus the immune response, enabling the elicitation of broadly neutralizing serological responses, as has been done with HIV-1 fusion peptide (Kong et al., 2019; Xu et al., 2018). Nanoparticles displaying the S2-helix may also be helpful in focusing the immune response, as has been done with the influenza stem site of vulnerability (Boyoglu-Barnum et al., 2021; Kanekiyo et al., 2013; Yassine et al., 2015). Whether

neutralization curves from two technical replicates of experiments are shown. Data are represented as mean percentages of neutralization with SEM calculated from the triplicate wells.

(B) Binding mode of WS6 is not compatible with the pre- and post-fusion conformations of the spike. The WS6-S2 peptide complex is superposed onto the pre- and post-fusion spike trimer by aligning the WS6-bound S2 peptide with the corresponding part in one of the protomers. S2-bound WS6 clashed with neighboring protomers in either pre- or post-fusion conformation, suggesting that binding disrupts pre-fusion conformation and prevents formation of post-fusion.

(C) Mechanism of neutralization by WS6. Structure of WS6 in complex with S2 peptide indicated that WS6 disrupts pre-fusion spike and prevents formation of the post-fusion conformation.

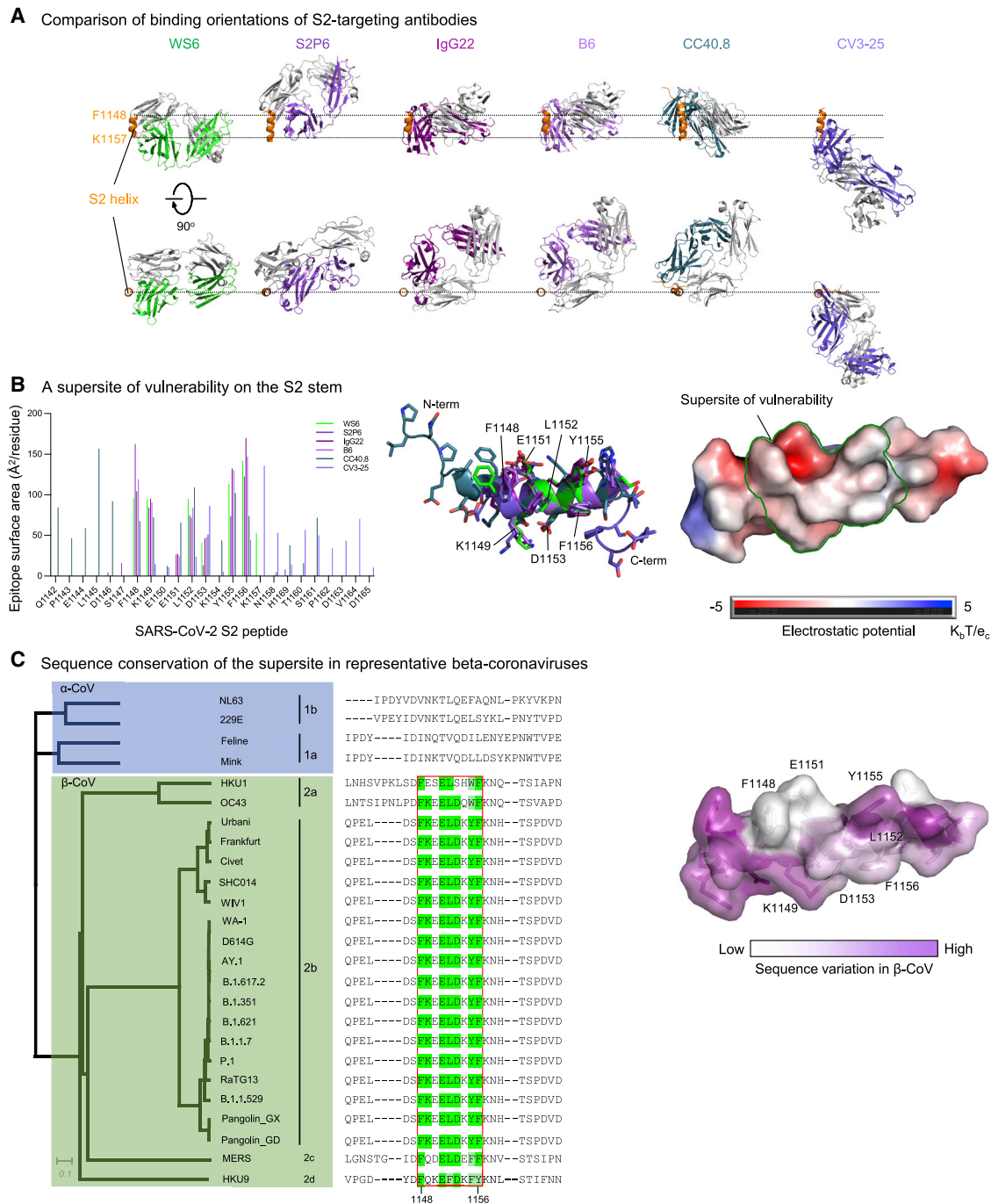


**Figure 5. An S2-stem supersite of vulnerability**

(A) Comparison of modes of recognition of WS6 with other antibodies targeting the S2 stem helix. WS6 binding to the S2 helix is shown in the same orientation as in Figure 4B. S2P6, IgG22, B6, and CV3-25 complexes are aligned with the WS6 complex over the S2 peptide helix. The S2 helix and light chains of antibodies are colored orange and gray, respectively. Heavy chains of antibodies are colored differently to distinguish them. CV3-25 assumes a distinct mode of recognition compared with others.

(B) Epitopes of antibodies targeting the S2 region define a supersite of vulnerability. Antibody-binding surface areas of each residue in the S2 peptide are plotted along the linear sequence of SARS-CoV-2 S2 peptide (left). Antibody-bound peptides are shown colored by recognizing antibodies. The center region between residues 1,148 and 1,156 is recognized by most of the antibodies (middle); hydrophobic residues F1148, L1152, Y1155, and F1156 are positioned in the middle of the supersite, with K1149, E1151, and D1153 providing hydrophilic interactions are the peripheral (right). The boundary of the supersite, which is defined as residues interacting with 5 of the 6 antibodies analyzed in this study, is highlighted by a green line.

(legend continued on next page)

S2-helix-focused immunization will elicit sufficiently broad and potent responses to enable protection from future SARS-CoV-2 variants or to future beta-coronavirus zoonotic crossovers remains to be seen. It seems likely that such immune focusing can be carried out in conjunction with spike-based immunizations, perhaps using currently licensed vaccines from Moderna, Pfizer, and Johnson and Johnson, all of which incorporate the S2-helical region.

## STAR★METHODS

Detailed methods are provided in the online version of this paper and include the following:

- **KEY RESOURCES TABLE**
- **RESOURCE AVAILABILITY**
  - Lead contact
  - Materials availability
  - Data and code availability
- **EXPERIMENTAL MODEL AND SUBJECT DETAILS**
  - Mouse studies
  - Cell lines
- **METHOD DETAILS**
  - Mouse immunization, hybridoma generation and antibody isolation
  - ELISA and dot-blot
  - Expression and purification of beta-coronavirus spike trimer proteins
  - Production of antibodies
  - Full-length spike constructs
  - Analysis of WS6 binding to cell surface expressed spike protein
  - Pseudovirus neutralization assay
  - Neutralization by fusion inhibition (post attachment inhibition)
  - Surface plasmon resonance measurements
  - Isothermal titration calorimetry (ITC)
  - Negative stain electron microscopy
  - Crystallization and structure determination
  - Antibody germline assignment
  - Antibody frequency calculation
  - Phylogenetic analysis
- **QUANTIFICATION AND STATISTICAL ANALYSIS**

## SUPPLEMENTAL INFORMATION

Supplemental information can be found online at <https://doi.org/10.1016/j.str.2022.06.004>.

## ACKNOWLEDGMENTS

We thank R. Andrabi for providing CC40.8 coordinates, B. Graham for suggesting use of flpin-TMPRSS2-ACE2 cells, T. Stephens for assistance with negative-stain EM, J. Stuckey for assistance with figures, and members of the Virology Laboratory, Vaccine Research Center, for discussions and comments on the manuscript. Support for this work was provided by the Intramural

Research Program of the Vaccine Research Center, National Institute of Allergy and Infectious Diseases, National Institutes of Health and by federal funds from the Frederick National Laboratory for Cancer Research under contract HHSN261200800001E. Use of sector 22 (Southeast Region Collaborative Access team) at the Advanced Photon Source was supported by the US Department of Energy, Basic Energy Sciences, Office of Science, under contract number W-31-109-Eng-38.

## AUTHOR CONTRIBUTIONS

W.S. isolated antibodies WS1–WS11 and performed ELISA binding assays; L.W. headed neutralization studies, prepared spike plasmids, and performed cell-surface binding assays; T.Z. determined and analyzed the crystal structure of the WS6-peptide complex and wrote the manuscript; M.S. performed SPR analysis, provided spike proteins for ELISA, and assisted with obtaining peptide for crystallization; E.S.Y., Y.Z., and M. Chen performed WS6 neutralization of SARS-related viruses; X.C. provided mouse next-generation sequencing (NGS) sequence data; M. Choe provided S2P6 antibody; A.C. provided 293 flpin-TMPRSS2-ACE2 cells; K.L. assisted with preparation of pseudoviruses; A.S.O. provided SARS-CoV-2 S2P-His for Octet measurements; A.P. and C.A.T. performed cell-surface staining; R.R. assisted with obtaining peptide for crystallization; A.S. performed ITC measurements; C.-H.S. prepared phylogenetic tree; E.-S.D.S. crystallized the protein complex; I-T.T. performed transfection for beta-CoV and S2 antibody productions; S.W. wrote the manuscript and performed PISA analysis of the antibody-peptide interface; K.S.C. carried out mouse immunization experiment; Y.T. performed negative-stain EM analysis; J.R.M. supervised antibody isolation, neutralization assessments, and cell-surface binding assays; P.D.K. oversaw the project and, with S.W. and T.Z., wrote the manuscript, with all authors providing comments or revisions.

## DECLARATION OF INTERESTS

The authors declare no competing interest.

Received: January 25, 2022

Revised: May 6, 2022

Accepted: June 21, 2022

Published: July 15, 2022

## REFERENCES

- Adams, P.D., Afonine, P.V., Bunkoczi, G., Chen, V.B., Davis, I.W., Echols, N., Headd, J.J., Hung, L.W., Kapral, G.J., Grosse-Kunstleve, R.W., et al. (2010). PHENIX: a comprehensive Python-based system for macromolecular structure solution. *Acta. Crystallogr. D Biol. Crystallogr.* **66**, 213–221.
- Albrecht, B., Scornavacca, C., Cenci, A., and Huson, D.H. (2012). Fast computation of minimum hybridization networks. *Bioinformatics* **28**, 191–197.
- Araf, Y., Akter, F., Tang, Y.D., Fatemi, R., Parvez, M.S.A., Zheng, C., and Hossain, M.G. (2022). Omicron variant of SARS-CoV-2: genomics, transmissibility, and responses to current COVID-19 vaccines. *J. Med. Virol.* **94**, 1825–1832.
- Barnes, C.O., West, A.P., Jr., Huey-Tubman, K.E., Hoffmann, M.A.G., Sharaf, N.G., Hoffman, P.R., Koranda, N., Gristick, H.B., Gaebler, C., Muecksch, F., et al. (2020). Structures of human antibodies bound to SARS-CoV-2 spike reveal common epitopes and recurrent features of antibodies. *Cell* **182**, 828–842.e16.
- Barouch, D.H., Yang, Z.Y., Kong, W.P., Koriath-Schmitz, B., Sumida, S.M., Truitt, D.M., Kishko, M.G., Arthur, J.C., Miura, A., Mascola, J.R., et al. (2005). A human T-cell leukemia virus type 1 regulatory element enhances the immunogenicity of human immunodeficiency virus type 1 DNA vaccines in mice and nonhuman primates. *J. Virol.* **79**, 8828–8834.

(C) Sequence conservation of the SARS-CoV-2 supersite in beta-coronaviruses. Sequence dendrogram was calculated using full spike protein sequences (far left). Sequence alignment shown residues 1,142–1,165, recognized by supersite antibodies in (B) (left middle). The surface of S2 peptide is colored by sequence variation score with corresponding residues shown in sticks representation (right). See also [Figures S4](#) and [S6](#).

- Boyoglu-Barnum, S., Ellis, D., Gillespie, R.A., Hutchinson, G.B., Park, Y.J., Moin, S.M., Acton, O.J., Ravichandran, R., Murphy, M., Pettie, D., et al. (2021). Quadrivalent influenza nanoparticle vaccines induce broad protection. *Nature* 592, 623–628.
- Brouwer, P.J.M., Caniels, T.G., van der Straten, K., Snitselaar, J.L., Aldon, Y., Bangaru, S., Torres, J.L., Okba, N.M.A., Claireaux, M., Kerster, G., et al. (2020). Potent neutralizing antibodies from COVID-19 patients define multiple targets of vulnerability. *Science* 369, 643–650.
- Cai, Y., Zhang, J., Xiao, T., Peng, H., Sterling, S.M., Walsh, R.M., Jr., Rawson, S., Rits-Volloch, S., and Chen, B. (2020). Distinct conformational states of SARS-CoV-2 spike protein. *Science* 369, 1586–1592.
- Cao, Y., Su, B., Guo, X., Sun, W., Deng, Y., Bao, L., Zhu, Q., Zhang, X., Zheng, Y., Geng, C., et al. (2020). Potent neutralizing antibodies against SARS-CoV-2 identified by high-throughput single-cell sequencing of convalescent patients' B cells. *Cell* 182, 73–84.e16.
- Cerutti, G., Guo, Y., Zhou, T., Gorman, J., Lee, M., Rapp, M., Reddem, E.R., Yu, J., Bahna, F., Bimela, J., et al. (2021). Potent SARS-CoV-2 neutralizing antibodies directed against spike N-terminal domain target a single supersite. *Cell Host Microbe* 29, 819–833.e7.
- Collaborative Computational Project (1994). The CCP4 suite: programs for protein crystallography. *Acta Crystallogr. D Biol. Crystallogr.* 50, 760–763.
- Corbett, K.S., Edwards, D.K., Leist, S.R., Abiona, O.M., Boyoglu-Barnum, S., Gillespie, R.A., Himansu, S., Schafer, A., Ziwawo, C.T., DiPiazza, A.T., et al. (2020). SARS-CoV-2 mRNA vaccine design enabled by prototype pathogen preparedness. *Nature* 586, 567–571.
- Drosten, C., Gunther, S., Preiser, W., van der Werf, S., Brodt, H.R., Becker, S., Rabenau, H., Panning, M., Kolesnikova, L., Fouchier, R.A., et al. (2003). Identification of a novel coronavirus in patients with severe acute respiratory syndrome. *N. Engl. J. Med.* 348, 1967–1976.
- Edara, V.V., Manning, K.E., Ellis, M., Lai, L., Moore, K.M., Foster, S.L., Floyd, K., Davis-Gardner, M.E., Mantus, G., Nyhoff, L.E., et al. (2021). mRNA-1273 and BNT162b2 mRNA vaccines have reduced neutralizing activity against the SARS-CoV-2 Omicron variant. Preprint at bioRxiv. <https://doi.org/10.1101/2021.12.20.473557>.
- Emsley, P., and Cowtan, K. (2004). Coot: model-building tools for molecular graphics. *Acta Crystallogr. D Biol. Crystallogr.* 60, 2126–2132.
- Garcia-Beltran, W.F., St Denis, K.J., Hoelzemer, A., Lam, E.C., Nitido, A.D., Sheehan, M.L., Berrios, C., Ofoman, O., Chang, C.C., Hauser, B.M., et al. (2022). mRNA-based COVID-19 vaccine boosters induce neutralizing immunity against SARS-CoV-2 Omicron variant. *Cell* 185, 457–466.e4. <https://doi.org/10.1016/j.cell.2021.12.033>.
- Hsieh, C.L., Werner, A.P., Leist, S.R., Stevens, L.J., Falconer, E., Goldsmith, J.A., Chou, C.W., Abiona, O.M., West, A., Westendorf, K., et al. (2021). Stabilized coronavirus spike stem elicits a broadly protective antibody. *Cell Rep.* 37, 109929.
- Hurlburt, N.K., Homad, L.J., Sinha, I., Jennewein, M.F., MacCamy, A.J., Wan, Y.-H., Boonyaratankornkit, J., Sholukh, A.M., Zhou, P., Burton, D.R., et al. (2021). Structural definition of a pan-sarbecovirus neutralizing epitope on the spike S2 subunit. Preprint at bioRxiv. <https://doi.org/10.1101/2021.08.02.454829>.
- Jaenicke, L. (1974). A rapid micromethod for the determination of nitrogen and phosphate in biological material. *Anal. Biochem.* 61, 623–627.
- Ju, B., Zhang, Q., Ge, J., Wang, R., Sun, J., Ge, X., Yu, J., Shan, S., Zhou, B., Song, S., et al. (2020). Human neutralizing antibodies elicited by SARS-CoV-2 infection. *Nature* 584, 115–119.
- Kanekiyo, M., Wei, C.J., Yassine, H.M., McTamney, P.M., Boyington, J.C., Whittle, J.R., Rao, S.S., Kong, W.P., Wang, L., and Nabel, G.J. (2013). Self-assembling influenza nanoparticle vaccines elicit broadly neutralizing H1N1 antibodies. *Nature* 499, 102–106.
- Ke, Z., Oton, J., Qu, K., Cortese, M., Zila, V., McKeane, L., Nakane, T., Zivanov, J., Neufeldt, C.J., Cerikan, B., et al. (2020). Structures and distributions of SARS-CoV-2 spike proteins on intact virions. *Nature* 588, 498–502.
- Kong, R., Duan, H., Sheng, Z., Xu, K., Acharya, P., Chen, X., Cheng, C., Dings, A.S., Gorman, J., Sastry, M., et al. (2019). Antibody lineages with vaccine-induced antigen-binding hotspots develop broad HIV neutralization. *Cell* 178, 567–584.e19.
- Kong, R., Xu, K., Zhou, T., Acharya, P., Lemmin, T., Liu, K., Ozorowski, G., Soto, C., Taft, J.D., Bailer, R.T., et al. (2016). Fusion peptide of HIV-1 as a site of vulnerability to neutralizing antibody. *Science* 352, 828–833.
- Krissinel, E., and Henrick, K. (2007). Inference of macromolecular assemblies from crystalline state. *J. Mol. Biol.* 372, 774–797.
- Ksiazek, T.G., Erdman, D., Goldsmith, C.S., Zaki, S.R., Peret, T., Emery, S., Tong, S., Urbani, C., Comer, J.A., Lim, W., et al. (2003). A novel coronavirus associated with severe acute respiratory syndrome. *N. Engl. J. Med.* 348, 1953–1966.
- Larkin, M.A., Blackshields, G., Brown, N.P., Chenna, R., McGettigan, P.A., McWilliam, H., Valentin, F., Wallace, I.M., Wilm, A., Lopez, R., et al. (2007). Clustal W and clustal X version 2.0. *Bioinformatics* 23, 2947–2948.
- Lefranc, M.P., Giudicelli, V., Duroux, P., Jabado-Michaloud, J., Folch, G., Aouinti, S., Carillon, E., Duvergey, H., Houles, A., Paysan-Lafosse, T., et al. (2015). IMGT(R), the international ImMunoGeneTics information system(R) 25 years on. *Nucleic Acids Res.* 43, D413–D422.
- Li, W., Chen, Y., Prevost, J., Ullah, I., Lu, M., Gong, S.Y., Tauzin, A., Gasser, R., Vezina, D., Anand, S.P., et al. (2022). Structural basis and mode of action for two broadly neutralizing antibodies against SARS-CoV-2 emerging variants of concern. *Cell Rep.* 38, 110210.
- Li, Y., Ma, M.L., Lei, Q., Wang, F., Hong, W., Lai, D.Y., Hou, H., Xu, Z.W., Zhang, B., Chen, H., et al. (2021). Linear epitope landscape of the SARS-CoV-2 Spike protein constructed from 1,051 COVID-19 patients. *Cell Rep.* 34, 108915.
- Liu, L., Iketani, S., Guo, Y., Chan, J.F., Wang, M., Liu, L., Luo, Y., Chu, H., Huang, Y., Nair, M.S., et al. (2021). Striking antibody evasion manifested by the Omicron variant of SARS-CoV-2. *Nature* 602, 676–681. <https://doi.org/10.1038/s41586-021-04388-0>.
- Liu, L., Wang, P., Nair, M.S., Yu, J., Rapp, M., Wang, Q., Luo, Y., Chan, J.F., Sahi, V., Figueroa, A., et al. (2020). Potent neutralizing antibodies against multiple epitopes on SARS-CoV-2 spike. *Nature* 584, 450–456.
- Marcou, Q., Mora, T., and Walczak, A.M. (2018). High-throughput immune repertoire analysis with IGoR. *Nat. Commun.* 9, 561.
- McCallum, M., De Marco, A., Lempp, F.A., Tortorici, M.A., Pinto, D., Walls, A.C., Beltramello, M., Chen, A., Liu, Z., Zatta, F., et al. (2021). N-terminal domain antigenic mapping reveals a site of vulnerability for SARS-CoV-2. *Cell* 184, 2332–2347.e16.
- McCoy, A.J., Grosse-Kunstleve, R.W., Adams, P.D., Winn, M.D., Storoni, L.C., and Read, R.J. (2007). Phaser crystallographic software. *J. Appl. Crystallogr.* 40, 658–674.
- Naldini, L., Blomer, U., Gage, F.H., Trono, D., and Verma, I.M. (1996). Efficient transfer, integration, and sustained long-term expression of the transgene in adult rat brains injected with a lentiviral vector. *Proc. Natl. Acad. Sci. USA* 93, 11382–11388.
- Otwinowski, Z., and Minor, W. (1997). Processing of X-ray diffraction data collected in oscillation mode. *Methods Enzymol.* 276, 307–326.
- Pajon, R., Doria-Rose, N.A., Shen, X., Schmidt, S.D., O'Dell, S., McDanal, C., Feng, W., Tong, J., Eaton, A., Magliano, M., et al. (2022). SARS-CoV-2 Omicron variant neutralization after mRNA-1273 booster vaccination. *N. Engl. J. Med.* 386, 1088–1091.
- Pinto, D., Sauer, M.M., Czudnochowski, N., Low, J.S., Tortorici, M.A., Housley, M.P., Noack, J., Walls, A.C., Bowen, J.E., Guarino, B., et al. (2021). Broad betacoronavirus neutralization by a stem helix-specific human antibody. *Science* 373, 1109–1116.
- Punjani, A., Rubinstein, J.L., Fleet, D.J., and Brubaker, M.A. (2017). cryoSPARC: algorithms for rapid unsupervised cryo-EM structure determination. *Nat. Methods* 14, 290–296.
- Robbiani, D.F., Gaebler, C., Muecksch, F., Lorenzi, J.C.C., Wang, Z., Cho, A., Agudelo, M., Barnes, C.O., Gazumyan, A., Finkin, S., et al. (2020). Convergent antibody responses to SARS-CoV-2 in convalescent individuals. *Nature* 584, 437–442.

- Rogers, T.F., Zhao, F., Huang, D., Beutler, N., Burns, A., He, W.T., Limbo, O., Smith, C., Song, G., Woehl, J., et al. (2020). Isolation of potent SARS-CoV-2 neutralizing antibodies and protection from disease in a small animal model. *Science* 369, 956–963.
- Sauer, M.M., Tortorici, M.A., Park, Y.J., Walls, A.C., Homad, L., Acton, O.J., Bowen, J.E., Wang, C., Xiong, X., de van der Schueren, W., et al. (2021). Structural basis for broad coronavirus neutralization. *Nat. Struct. Mol. Biol.* 28, 478–486.
- Sethna, Z., Elhanati, Y., Callan, C.G., Walczak, A.M., and Mora, T. (2019). OLGA: fast computation of generation probabilities of B- and T-cell receptor amino acid sequences and motifs. *Bioinformatics* 35, 2974–2981.
- Seydoux, E., Homad, L.J., MacCamy, A.J., Parks, K.R., Hurlburt, N.K., Jennewein, M.F., Akins, N.R., Stuart, A.B., Wan, Y.H., Feng, J., et al. (2020). Analysis of a SARS-CoV-2-infected individual reveals development of potent neutralizing antibodies with limited somatic mutation. *Immunity* 53, 98–105.e5.
- Sievers, B.L., Chakraborty, S., Xue, Y., Gelbart, T., Gonzalez, J.C., Cassidy, A.G., Golan, Y., Prah, M., Gaw, S.L., Arunachalam, P.S., et al. (2022). Antibodies elicited by SARS-CoV-2 infection or mRNA vaccines have reduced neutralizing activity against Beta and Omicron pseudoviruses. *Sci. Transl. Med.* 14, eabn7842. <https://doi.org/10.1126/scitranslmed.abn7842>.
- Suryadevara, N., Shrihari, S., Gilchuk, P., VanBlargan, L.A., Binshtein, E., Zost, S.J., Nargi, R.S., Sutton, R.E., Winkler, E.S., Chen, E.C., et al. (2021). Neutralizing and protective human monoclonal antibodies recognizing the N-terminal domain of the SARS-CoV-2 spike protein. *Cell* 184, 2316–2331.e15.
- Syed, A.M., Ciling, A., Khalid, M.M., Sreekumar, B., Chen, P.Y., Kumar, G.R., Silva, I., Milbes, B., Kojima, N., Hess, V., et al. (2022). Omicron mutations enhance infectivity and reduce antibody neutralization of SARS-CoV-2 virus-like particles. Preprint at medRxiv. <https://doi.org/10.1101/2021.12.20.21268048>.
- Wang, C., van Haperen, R., Gutierrez-Alvarez, J., Li, W., Okba, N.M.A., Albulescu, I., Widjaja, I., van Dieren, B., Fernandez-Delgado, R., Sola, I., et al. (2021a). A conserved immunogenic and vulnerable site on the coronavirus spike protein delineated by cross-reactive monoclonal antibodies. *Nat. Commun.* 12, 1715.
- Wang, L., Zhou, T., Zhang, Y., Yang, E.S., Schramm, C.A., Shi, W., Pegu, A., Oloniniyi, O.K., Henry, A.R., Darko, S., et al. (2021b). Ultrapotent antibodies against diverse and highly transmissible SARS-CoV-2 variants. *Science* 373, eabh1766.
- Williams, C.J., Headd, J.J., Moriarty, N.W., Prisant, M.G., Videau, L.L., Deis, L.N., Verma, V., Keedy, D.A., Hintze, B.J., Chen, V.B., et al. (2018). MolProbity: more and better reference data for improved all-atom structure validation. *Protein Sci.* 27, 293–315.
- Wrapp, D., Wang, N., Corbett, K.S., Goldsmith, J.A., Hsieh, C.L., Abiona, O., Graham, B.S., and McLellan, J.S. (2020). Cryo-EM structure of the 2019-nCoV spike in the prefusion conformation. *Science* 367, 1260–1263.
- Wu, X., Zhou, T., Zhu, J., Zhang, B., Georgiev, I., Wang, C., Chen, X., Longo, N.S., Louder, M., McKee, K., et al. (2011). Focused evolution of HIV-1 neutralizing antibodies revealed by structures and deep sequencing. *Science* 333, 1593–1602.
- Xu, K., Acharya, P., Kong, R., Cheng, C., Chuang, G.Y., Liu, K., Louder, M.K., O'Dell, S., Rawi, R., Sastry, M., et al. (2018). Epitope-based vaccine design yields fusion peptide-directed antibodies that neutralize diverse strains of HIV-1. *Nat. Med.* 24, 857–867.
- Yassine, H.M., Boyington, J.C., McTamney, P.M., Wei, C.J., Kanekiyo, M., Kong, W.P., Gallagher, J.R., Wang, L., Zhang, Y., Joyce, M.G., et al. (2015). Hemagglutinin-stem nanoparticles generate heterosubtypic influenza protection. *Nat. Med.* 21, 1065–1070.
- Zaki, A.M., van Boheemen, S., Bestebroer, T.M., Osterhaus, A.D., and Fouchier, R.A. (2012). Isolation of a novel coronavirus from a man with pneumonia in Saudi Arabia. *N. Engl. J. Med.* 367, 1814–1820.
- Zhou, P., Yang, X.L., Wang, X.G., Hu, B., Zhang, L., Zhang, W., Si, H.R., Zhu, Y., Li, B., Huang, C.L., et al. (2020a). A pneumonia outbreak associated with a new coronavirus of probable bat origin. *Nature* 579, 270–273.
- Zhou, P., Yuan, M., Song, G., Beutler, N., Shaabani, N., Huang, D., He, W.T., Zhu, X., Callaghan, S., Yong, P., et al. (2021). A protective broadly cross-reactive human antibody defines a conserved site of vulnerability on beta-coronavirus spikes. Preprint at bioRxiv. <https://doi.org/10.1101/2021.03.30.437769>.
- Zhou, T., Teng, I.T., Ollia, A.S., Cerutti, G., Gorman, J., Nazzari, A., Shi, W., Tsybovsky, Y., Wang, L., Wang, S., et al. (2020b). Structure-based design with tag-based purification and in-process biotinylation enable streamlined development of SARS-CoV-2 spike molecular probes. *Cell Rep.* 33, 108322.
- Zhu, N., Zhang, D., Wang, W., Li, X., Yang, B., Song, J., Zhao, X., Huang, B., Shi, W., Lu, R., et al. (2020). A novel coronavirus from patients with pneumonia in China, 2019. *N. Engl. J. Med.* 382, 727–733.
- Zost, S.J., Gilchuk, P., Chen, R.E., Case, J.B., Reidy, J.X., Trivette, A., Nargi, R.S., Sutton, R.E., Suryadevara, N., Chen, E.C., et al. (2020). Rapid isolation and profiling of a diverse panel of human monoclonal antibodies targeting the SARS-CoV-2 spike protein. *Nat. Med.* 26, 1422–1427.

STAR★METHODS

KEY RESOURCES TABLE

REAGENT or RESOURCE	SOURCE	IDENTIFIER
<b>Antibodies</b>		
WS1	This paper	N/A
WS2	This paper	N/A
WS3	This paper	N/A
WS4	This paper	N/A
WS5	This paper	N/A
WS6	This paper	N/A
WS7	This paper	N/A
WS8	This paper	N/A
WS9	This paper	N/A
WS10	This paper	N/A
WS11	This paper	N/A
Mouse IgG1	ThermoFisher Scientific	Cat# 02-6100
S2P6	<a href="#">Pinto et al., 2021</a>	N/A
<b>Bacterial and virus strains</b>		
SARS-CoV-2 WA-1 pseudovirus	<a href="#">Wang et al., 2021b</a>	N/A
SARS-CoV-2 D614G pseudovirus	<a href="#">Wang et al., 2021b</a>	N/A
SARS-CoV-2 B.1.1.7 pseudovirus	<a href="#">Wang et al., 2021b</a>	N/A
SARS-CoV-2 B.1.351 pseudovirus	<a href="#">Wang et al., 2021b</a>	N/A
SARS-CoV-2 P.1 pseudovirus	<a href="#">Wang et al., 2021b</a>	N/A
SARS-CoV-2 B.1.617.2 pseudovirus	<a href="#">Wang et al., 2021b</a>	N/A
SARS-CoV-2 AY.1 pseudovirus	This paper	N/A
SARS-CoV-2 B.1.621 pseudovirus	This paper	N/A
SARS-CoV-2 B.1.1.529 pseudovirus	This paper	N/A
SARS-CoV pseudovirus	This paper	N/A
RaTG13 pseudovirus	This paper	N/A
Pangolin-GD pseudovirus	This paper	N/A
Pangolin-GX pseudovirus	This paper	N/A
Frankfurt pseudovirus	This paper	N/A
Civet 007-2004 pseudovirus	This paper	N/A
WIV1 pseudovirus	This paper	N/A
SHC014 pseudovirus	This paper	N/A
MERS-CoV pseudovirus	This paper	N/A
hCoV-229E pseudovirus	This paper	N/A
<b>Chemicals, peptides, and recombinant proteins</b>		
Complete His-Tag Resin	Roche	Cat# 05893801001
HEPES	Life Technologies	Cat# 15630-080
IgG elution buffer	Thermo Scientific	Cat# 21009
Luciferase assay reagent	Promega	Cat# E1500
Ni-NTA Capture Biosensors	fortéBIO	Cat# 18-5103
Recombinant Protein A Sepharose	GE Healthcare	Cat# 17-1279-03
Sodium chloride	Quality Biological, Inc	Cat# 351-036-101
Turbo293 transfection reagent	SPEED BioSystem	Cat# PXX1002
SARS-CoV spike peptide array	BEI Resources	Cat# NR-52418
S2 peptide: Ac-FKEELDKYFK-biotin-PEG	GenScript	N/A

(Continued on next page)

**Continued**

REAGENT or RESOURCE	SOURCE	IDENTIFIER
hCoV-HKU1 S2P	This paper	N/A
MERS-CoV S2P	This paper	N/A
hCoV-OC43 S2P	This paper	N/A
RaTG13 S2P	This paper	N/A
SARS-CoV S2P	This paper	N/A
SARS-CoV-2 S1-short	This paper	N/A
SARS-CoV-2 S1R	This paper	N/A
SARS-CoV-2 S2P	<a href="#">Wrapp et al., 2020</a>	N/A
SARS-CoV-2 S-dTM	This paper	N/A
SARS-CoV-2 WA-1 spike	This paper	N/A
SHC014 S2P	This paper	N/A
WIV1 S2P	This paper	N/A
<b>Critical commercial assays</b>		
DNA gene synthesis and cloning	GenScript Biotech Corporation	N/A
Site-directed mutagenesis	Genelimmune Biotechnology LLC	N/A
Fab kit	Pierce	Cat# 44985
Rapid isotyping kit	Pierce	Cat# 26178
QuikChange multisite-directed mutagenesis kit	Agilent	Cat# 210515
<b>Deposited data</b>		
Crystal structure of WS6 in complex with S2 peptide	This paper	PDB: 7TCQ
<b>Experimental models: Cell lines</b>		
Human: Expi293F cells	Thermo Fisher	Cat# A14527; RRID: CVCL_D615
Human: FreeStyle 293-F cells	Thermo Fisher	Cat# R79007
<b>Recombinant DNA</b>		
pVRC8400-full-length spike Civet 007-2004	This paper	GenBank ID: AAU04646.1
pVRC8400-full-length spike Frankfurt1	This paper	GenBank ID: BAE93401.1
pVRC8400-full-length spike hCoV-229E	This paper	GenBank ID: AOG74783.1
pVRC8400-full-length spike hCoV-HKU1	This paper	GenBank ID: AAT98580.1
pVRC8400-full-length spike hCoV-OC43	This paper	GenBank ID: AAT84354.1
pVRC8400-full-length spike MERS-CoV	This paper	GenBank ID: AFS88936
pVRC8400-full-length spike Pangolin_GD	This paper	GenBank ID: QIA48632.1
pVRC8400-full-length spike Pangolin_GX	This paper	GenBank ID: QIQ54048.1
pVRC8400-full-length spike RaTG13	This paper	GenBank ID: QHR63300.2
pVRC8400-full-length spike SARS-CoV-2	This paper	GenBank ID: QHD43416.1
pVRC8400-full-length spike SARS-CoV	This paper	GenBank ID: AAP13441.1
pVRC8400-full-length spike SARS-CoV-2 D614G	This paper	N/A
pVRC8400-full-length spike SARS-CoV-2 AY.1	This paper	N/A
pVRC8400-full-length spike SARS-CoV-2 B.1.1.7	This paper	N/A
pVRC8400-full-length spike SARS-CoV-2 B.1.1.529	This paper	N/A
pVRC8400-full-length spike SARS-CoV-2 B.1.351	This paper	N/A
pVRC8400-full-length spike SARS-CoV-2 B.1.617.2	This paper	N/A
pVRC8400-full-length spike SARS-CoV-2 B.1.621	This paper	N/A
pVRC8400-full-length spike SARS-CoV-2 P.1	This paper	N/A
pVRC8400-full-length spike SHC014	This paper	GenBank ID: KC881005
pVRC8400-full-length spike WIV1	This paper	GenBank ID: KF367457
pVRC8400-WS6-heavy-chain	This paper	N/A
pVRC8400-WS6-light-chain	This paper	N/A

(Continued on next page)

**Continued**

REAGENT or RESOURCE	SOURCE	IDENTIFIER
Software and algorithms		
Biacore T200 evaluation software	Cytiva	<a href="https://www.cytivalifesciences.com/en/us/shop/protein-analysis/spr-label-free-analysis/software">https://www.cytivalifesciences.com/en/us/shop/protein-analysis/spr-label-free-analysis/software</a>
CCP4 Program Suite	Collaborative Computational Project, 1994	<a href="https://www.ccp4.ac.uk">https://www.ccp4.ac.uk</a>
ClustalW	Larkin et al., 2007	<a href="https://www.ebi.ac.uk/Tools/msa/clustalo/">https://www.ebi.ac.uk/Tools/msa/clustalo/</a>
Coot	Emsley and Cowtan, 2004	<a href="https://sbgrid.org/software/">https://sbgrid.org/software/</a>
CryoSPARC 2.15	Punjani et al., 2017	<a href="https://cryosparc.com">https://cryosparc.com</a>
Dendroscope	Albrecht et al., 2012	<a href="https://software-ab.informatik.uni-tuebingen.de/download/dendroscope3/welcome.html">https://software-ab.informatik.uni-tuebingen.de/download/dendroscope3/welcome.html</a>
HKL2000	Otwinowski and Minor, 1997	<a href="https://hkl-xray.com">https://hkl-xray.com</a>
IMGT	Lefranc et al., 2015	<a href="http://www.imgt.org">http://www.imgt.org</a>
MolProbity	Williams et al., 2018	<a href="http://molprobity.biochem.duke.edu">http://molprobity.biochem.duke.edu</a>
Origin	Malvern Panalytical	<a href="https://www.origin.com/usa/en-us/store/download">https://www.origin.com/usa/en-us/store/download</a>
PDBePISA	Krissinel and Henrick, 2007	<a href="http://www.ebi.ac.uk/pdbe/pisa/">http://www.ebi.ac.uk/pdbe/pisa/</a>
Phenix	Adams et al., 2010	<a href="https://sbgrid.org/software/">https://sbgrid.org/software/</a>
PRISM	GraphPad Software	<a href="https://www.graphpad.com/scientific-software/prism/">https://www.graphpad.com/scientific-software/prism/</a>
PyMOL	Schrödinger	<a href="https://pymol.org">https://pymol.org</a>

**RESOURCE AVAILABILITY**

**Lead contact**

Further information and requests for resources and reagents should be directed to and will be fulfilled by the Lead Contact, Peter D. Kwong ([pdkwong@nih.gov](mailto:pdkwong@nih.gov)).

**Materials availability**

Plasmids generated in this study are available upon request.

**Data and code availability**

- Crystal diffraction data and structure coordinates of WS6 in complex have been deposited with the Protein Data Bank, PDB: 7TCQ, <https://doi.org/10.2210/pdb7tcq/pdb>.
- This paper does not report original code.
- Any additional information required to reanalyze the data reported in this paper is available from the [lead contact](#) upon request.

**EXPERIMENTAL MODEL AND SUBJECT DETAILS**

**Mouse studies**

Animal experiments were carried out in compliance with all pertinent US National Institutes of Health regulations and approval from the Animal Care and Use Committee (ACUC) of the Vaccine Research Center. BALB/cJ mice (Jackson Laboratory), 6- to 8-week-old female, were used.

**Cell lines**

FreeStyle 293-F (cat# R79007) and Expi293F cells (cat# A14528; RRID: CVCL\_D615) were purchased from ThermoFisher Scientific Inc. FreeStyle 293-F cells were maintained in FreeStyle 293 Expression Medium, while Expi293F cells were maintained in Expi Expression Medium. The above cell lines were used directly from the commercial sources and cultured according to manufacturer suggestions.

**METHOD DETAILS**

**Mouse immunization, hybridoma generation and antibody isolation**

Female Balb/c mice were immunized with mRNA encoding for SARS-CoV-2 full-length spike from the wildtype WA-1 strain at weeks 0 and 3. Each animal received 1 µg mRNA diluted in 50 µl of 1xPBS via intramuscular injection into the same hind leg for both prime and

boost, utilizing methods described previously (Corbett et al., 2020). Serum samples were collected to detect antibody responses. One mouse with the best neutralizing antibody titer against SARS-CoV-2 spike was boosted intravenously with 20  $\mu\text{g}$  of SARS-CoV-2 S-dTM (wild type spike with transmembrane region deleted, aa 1-1206) at week 12. Three days later, splenocytes were harvested and fused with Sp2/0 myeloma cells (ATCC) using polyethylene glycol (PEG) 1450 (50% (w/v), Sigma-Aldrich) according to the standard methods. Cells were cultured and screened in RPMI complete medium that contained 20% FCS and  $1 \times 100 \mu\text{M}$  hypoxanthine,  $0.4 \mu\text{M}$  aminopterin and  $16 \mu\text{M}$  thymidine (Sigma-Aldrich). Supernatants from resulting hybridomas were screened for binding, using ELISA, to SARS-CoV-2 S1, NTD, RBD or S-dTM as well as for neutralizing activity. Subclones were generated by limiting dilution. After three rounds of screening and subcloning, stable antibody-producing clones were isolated and adapted to hybridoma-serum-free medium (Life Technologies Corp., Grand Island, NY, USA). Supernatants were collected from selected hybridoma clones and purified through a protein G-sepharose column (GE Healthcare). Monoclonal antibodies were isotyped with Pierce rapid isotyping kit (Cat#26178). Fabs were generated using Pierce Fab kit (Cat#44985) following manufacturer's instructions. Antibody and Fab purity was confirmed by SDS-PAGE. Select hybridomas were sent to GenScript (Piscataway, NJ 08854, USA) for hybridoma heavy and light chain variable sequences and IMGT (Lefranc et al., 2015) analysis.

### ELISA and dot-blot

ELISA plates were coated with the SARS-CoV-2 proteins, S-dTM, S1-short (residues 1-670), S1R (residues 1-537), RBD, and NTD, at  $1 \mu\text{g/ml}$  in PBS at  $4^\circ\text{C}$  overnight. After standard washes and blocks, plates were incubated with  $50 \mu\text{l}$  serial dilutions of antibody in each well for one hour at room temperature. Anti-mouse whole IgG horseradish peroxidase conjugates (Jackson Laboratory) were used as secondary antibodies, and 3,5,3',5'-tetramethylbenzidine (TMB) (KPL, Gaithersburg, MD) was used as the substrate.

To identify WS6 epitope, a dot-blot was performed. SARS-CoV spike peptide array (NR-52418), was purchased from BEI resource.  $20 \text{ ng}$  of each of the 78 peptides (#91-169) covering the SARS-CoV spike S2 region were dotted on a nitrocellulose membrane. SARS-CoV-2 RBD, S2, S-dTM and S2P proteins were also dotted on the membrane as controls. Non-specific sites were blocked by soaking in PBS-Tween 20 containing 5% dry milk. The membrane was washed three times with PBS-T buffer, then incubated with  $2 \mu\text{g/ml}$  of antibody WS6 in blocking buffer for one hour at room temperature. After washing three times with PBS-T buffer, the membrane was incubated 30 min with anti-mouse IgG horseradish peroxidase conjugates (Jackson Laboratory) as secondary antibody. The membrane was then developed with ECL medium.

### Expression and purification of beta-coronavirus spike trimer proteins

Diverse beta-coronavirus spike soluble proteins were stabilized in prefusion conformation by double-proline (2P) mutations corresponding to K986P and V987P in SARS CoV-2 spike protein, along with a T4-phage fibrin trimerization domain (foldon) at the C terminus (Wrapp et al., 2020) followed by an HRV3C cleavage site, His<sub>8</sub> and Twin-Streptactin purification tags. Additionally, the furin cleavage sites between S1 and S2 were mutated; for HKU1 and OC43, RRRKR was replaced by GGSGG; for MERS-CoV, RSVR was replaced with ASVG; for SARS-CoV, SHC014, WIV1, and RaTG13, SLLRST was replaced with SLLAST. DNA sequences encoding diverse beta-coronavirus S2P proteins with T4-foldon motif, His<sub>8</sub> and Twin-Streptactin purification tags were cloned into mammalian expression vector pVRC8400 by GeneImmune. These stabilized S2P proteins were expressed by transient transfection of FreeStyle 293-F cells as previously described (Zhou et al., 2020b). Specifically,  $1 \text{ mg}$  of transfection grade plasmid DNA and  $3 \text{ ml}$  of Turbo293 transfection reagent (Speed BioSystems) each in  $20 \text{ ml}$  Opti-MEM (Thermo Fisher Scientific), were pre-mixed and transfected into FreeStyle 293-F cells. Transfected cells were grown for 6 days at  $120 \text{ rpm}$ ,  $37^\circ\text{C}$ , and 9%  $\text{CO}_2$ , and the supernatant was harvested by centrifugation to remove cell debris. Supernatants were sterile-filtered, and the spike trimers were purified by nickel affinity chromatography using cOmplete His-Tag purification resin. The resin was serially washed with  $50 \text{ mM}$  Tris, pH 8.0,  $400 \text{ mM}$  NaCl buffer containing  $10 \text{ mM}$  and  $25 \text{ mM}$  Imidazole, respectively. The proteins were eluted in  $50 \text{ mM}$  Tris, pH 8.0,  $400 \text{ mM}$  NaCl,  $300 \text{ mM}$  Imidazole. Protein fractions were pooled and further purified by size-exclusion chromatography using a Superdex 200 16/600 column (Cytiva) in PBS. Fractions corresponding to trimeric spike proteins were pooled, concentrated to  $1 \text{ mg/ml}$ , analyzed by SDS-PAGE and stored at  $-80^\circ\text{C}$  until further use.

### Production of antibodies

Monoclonal antibody WS6 heavy and light chain variable regions were cloned from WS6 hybridoma cells and sequenced. The heavy and light chain variable region sequences were synthesized with codon optimized for human cell expression and then subcloned into corresponding pVRC8400 vectors containing mouse IgG1 heavy chain and kappa light chain constant regions by GenScript (Piscataway, NJ). All other antibody heavy and light variable region gene sequences were synthesized by Gene Universal Inc (Newark, DE) and subcloned into corresponding pVRC8400 vectors containing human or mouse IgG1, kappa, or lambda constant region and a human cytomegalovirus promoter. The resulting plasmids of heavy and light chain pairs were co-transfected in Expi293F cells (Thermo Fisher) using Turbo293 transfection reagent (Speed BioSystems) as described previously (Wu et al., 2011). Briefly,  $500 \mu\text{g}$  plasmid encoding heavy-chain and  $500 \mu\text{g}$  plasmid encoding light-chain variant genes were pre-mixed with  $3 \text{ ml}$  of the transfection reagent for per  $1 \text{ L}$  of transfection. Cells were transfected at density of  $2.5 \times 10^6/\text{ml}$  followed by incubation in a shaker incubator at  $120 \text{ rpm}$ ,  $37^\circ\text{C}$ , 9%  $\text{CO}_2$ . On day 5 post transfection, the culture supernatants were harvested, sterile filtered and loaded onto a protein A column. The columns were washed with PBS, and IgG proteins were eluted with a low pH IgG elution buffer (Pierce) and immediately neutralized with  $1 \text{ M}$  Tris-HCl, pH 8.0. Purified IgGs were subsequently dialyzed twice against PBS pH 7.4 using  $10 \text{ kD}$  dialysis cartridges (Pierce) and used for all measurements.

### Full-length spike constructs

Codon optimized cDNAs encoding full-length spike from SARS-CoV-2 (GenBank ID: QHD43416.1) were synthesized, cloned into the mammalian expression vector VRC8400 (Barouch et al., 2005) and confirmed by sequencing. Spike containing D614G amino acid change was generated using the wildtype spike sequence. Other variants containing single or multiple amino-acid changes in the spike gene from wildtype or D614G were made by mutagenesis using QuickChange lightning Multi Site-Directed Mutagenesis Kit (cat # 210515, Agilent) or via synthesis and cloning (Genscript). The spike variants tested are B.1.1.7 ( H69del-V70del-Y144del-N501Y-A570D-D614G-P681H-T716I-S982A-D1118H), B.1.351 (L18F-D80A-D215G-(L242-244)del-R246I-K417N-E484K-N501Y-A701V), P.1 (L18F-T20N-P26S-D138Y-R190S-K417T-E484K-N501Y-D614G-H655Y-T1027I-V1176F), B.1.617.2 ( T19R, G142D, del156-157, R158G, L452R, T478K, D614G, P681R, D950N), AY.1 (T19R, T95I, G142D, E156del, F157del, R158G, W258L, K417N, L452R, T478K, D614G, P681R, D950N), B.1.621 (T95I, insert144T, Y144S, Y145N, R346K, E484K, N501Y, D614G, P681H, D950N) and B.1.1.529 ( A67V, H69del, V70del, T95I, G142D, V143del, Y144del, Y145del, N211del, L212I, ins214EPE, G339D, S371L, S373P, S375F, K417N, N440K, G446S, S477N, T478K, E484A, Q493R, G496S, Q498R, N501Y, Y505H, T547K, D614G, H655Y, N679K, P681H, N764K, D796Y, N856K, Q954H, N969K, L981F). The spike genes from SARS-CoV-2 related CoVs (RaTG13\_GenBank: QHR63300.2; Pangolin GD\_GenBank: QIA48632.1; Pangolin\_GX-P2V\_QIQ54048.1), SARS-CoV and related CoVs (SARS-CoV Urbani\_GenBank: AAP13441.1; Frankfurt1\_GenBank: BAE93401.1; Civet SARS CoV 007/2004 S\_GenBank: AAU04646.1; WIV1\_GenBank: KF367457; SHC014\_GenBank: KC881005), MERS-CoV EMC\_GenBank: AFS88936), hCoV-HKU1 (GenBank: AAT98580.1), hCoV-OC43 (GenBank: AAT84354.1) and hCoV-229E (GenBank: AOG74783.1) were synthesized (Genscript). These full-length spike plasmids were used for pseudovirus production and for cell surface binding assays.

### Analysis of WS6 binding to cell surface expressed spike protein

Expi-293 cells were transiently transfected with plasmids encoding full-length spike proteins of coronaviruses using Turbo293 transfection reagent (Speed BioSystems) following manufacturer's protocol. After 40 h, cells were harvested and incubated with monoclonal antibodies (1  $\mu$ g/mL) for 30 min. Cells were washed and incubated with an allophycocyanin conjugated anti-human IgG (709-136-149, Jackson ImmunoResearch Laboratories) for another 30 min, then washed and fixed with 1% paraformaldehyde (15712-S, Electron Microscopy Sciences). Flow cytometry data were acquired in a BD LSRFortessa X-50 flow cytometer (BD biosciences) and analyzed using Flowjo (BD biosciences).

### Pseudovirus neutralization assay

Spike-containing lentiviral pseudovirions were produced by co-transfection of packaging plasmid pCMVdr8.2, transducing plasmid pHR' CMV-Luc, a TMPRSS2 plasmid and S plasmids from human and animal coronaviruses (SARS-CoV-2 variants, SARS-CoV, MERS-CoV and SARS-CoV-2, SARS-CoV related coronaviruses) into 293T cells using Lipofectamine 3000 transfection reagent (L3000-001, ThermoFisher Scientific, Asheville, NC) (Naldini et al., 1996). 293T-ACE2 cells (provided by Dr. Michael Farzan) or 293 flpin-TMPRSS2-ACE2 cells (made at the VRC) were used for neutralization assay for SARS-CoV-2, SARS-CoV, and related sarbecoviruses while Huh7.5 cells (provided by Dr. Deborah R. Taylor) for MERS-CoV and hCoV-229E. Cells were plated into 96-well white/black Isoplates (PerkinElmer, Waltham, MA) at 75,000 cells per well the day before infection of pseudovirus. Serial dilutions of antibody were mixed with titrated pseudovirus, incubated for 45 min at 37°C and added to cells in triplicate. Following 2 h of incubation, wells were replenished with 150  $\mu$ l of fresh media. Cells were lysed 72 h later, and luciferase activity was measured with Microbeta (Perkin Elmer). Percent neutralization was calculated as  $100 \times ((\text{virus only control}) - (\text{virus plus antibody})) / (\text{virus only control})$ . Dose-response curves were generated with a 5-parameter nonlinear function using GraphPad Prism 8.0.2, and titers reported as the antibody concentration required to achieve 50% (50% inhibitory concentration [IC50]) or 80% (80% inhibitory concentration [IC80]) neutralization ratio [IC50] or 80% (80% inhibitory concentration [IC80]) neutralization.

### Neutralization by fusion inhibition (post attachment inhibition)

BHK21-ACE2 or 293 flpin-TMPRSS2-ACE2 cells were placed on ice for one hour before incubating with SARS-CoV-2 spike pseudotyped lentivirus on ice for another hour to allow the virus to attach to ACE2. After three washes, cells were then incubated with antibody on ice for additional one hour before further incubation. Cells were lysed after 72 h, and luciferase activity was measured with Microbeta (Perkin Elmer). Percent neutralization, neutralization IC50s, and IC80s were calculated using GraphPad Prism 8.0.2.

### Surface plasmon resonance measurements

Binding affinities and kinetics of WS6 antibody Fab to the His-tagged Diverse CoV S2P spike trimers were assessed by surface plasmon resonance (SPR) on a Biacore S-200 (GE Healthcare) at 25 °C. Affinity was measured on a Ni-NTA sensor chip (Cytiva). The Ni-NTA surface was activated by injection of 5 mM of Ni<sub>2</sub>SO<sub>4</sub> in HBS-EP+ buffer (10 mM HEPES, pH 7.4, 150 mM NaCl, 50  $\mu$ M EDTA and 0.05% surfactant P-20) for 60 s at 10  $\mu$ L/min and then stabilized by washing with HBS-EP+ buffer containing 50  $\mu$ M EDTA for 60 s at 30  $\mu$ L/min. Diverse CoV trimer S2P proteins with His-tag at 10  $\mu$ g/mL were captured at 6  $\mu$ L/min flow rate for 80 s over the nickel-activated sensor surface. Binding affinities for the captured trimer were determined using a serial dilution of antibody Fab solutions starting at 1600 nM during the association phase. A dissociation phase at 30  $\mu$ L/min for 1000 s was

used to determine binding kinetics. The surface was regenerated by flowing 250 mM imidazole to both channels at 50  $\mu\text{L}/\text{min}$  for 60 s. Sensorgrams of the concentration series were corrected with corresponding blank curves and fitted globally with Biacore S200 evaluation software using a 1:1 Langmuir model of binding.

### Isothermal titration calorimetry (ITC)

Calorimetric titration experiments were performed using a MicroCal VP-ITC microcalorimeter from Malvern Panalytical (Northampton, MA, USA). The calorimetric cell (volume  $\sim 1.4$  mL) was filled with S2P protein at 0.5  $\mu\text{M}$  (expressed per trimer) or peptide at 1  $\mu\text{M}$ . The WS6 antibody, prepared at a concentration of 12–14  $\mu\text{M}$  (expressed per antigen binding site), was injected in aliquots of 10  $\mu\text{L}$  with 300 seconds interval. The reactants were dissolved in PBS, pH 7.4, and all measurements were performed at 25  $^{\circ}\text{C}$ . The concentrations of WS6 and S2P protein were obtained from the absorbance at 280 nm while the exact concentrations of the peptides were obtained by total nitrogen determination (Jaenicke, 1974). The data were processed with Origin. The heat produced upon injection was obtained by integration of the calorimetric signal,  $dQ/dt$ . The heat associated with binding of the antibody was obtained by subtracting the heat of dilution from the heat of reaction. The values for the enthalpy change,  $\Delta H$ , the association constant,  $K_a$  (the dissociation constant,  $K_D = 1/K_a$ ) and the stoichiometry,  $N$ , were obtained by a nonlinear fit of the data to a single-site binding model. Gibbs energy,  $\Delta G$ , was calculated from the relation  $\Delta G = -RT \ln K_a$ , where  $T$  is the absolute temperature in kelvin and  $R$  the universal gas constant, (1.987 cal/(K  $\times$  mol)). The entropy contribution to Gibbs energy,  $-T\Delta S$ , was calculated from the known relation  $\Delta G = \Delta H - T\Delta S$ . The results were expressed per mole of antigen binding sites. The stoichiometry,  $N$ , denotes the number of antigen binding sites per mole S2P trimer or peptide.

### Negative stain electron microscopy

Protein complex of WS6 Fab and SARS-CoV-2 spike was formed by mixing the Fab and spike protein at 1.2:1 molar ratio and incubating at room temperature for 15 minutes. The protein mixture was then diluted to about 0.02 mg/ml, adsorbed to freshly glow-discharged carbon-film grids for 15 s, washed with a buffer containing 20 mM HEPES, pH 7.5, and 150 mM NaCl, and stained with 0.7% uranyl formate, pH 5. Datasets were collected on a Thermo Scientific Talos F200C transmission electron microscope equipped with a Ceta camera at 200 kV,  $-1.2$   $\mu\text{m}$  defocus and 57,000 $\times$  nominal magnification which corresponds to a pixel size of 2.53  $\text{\AA}$ . Data was collected automatically using EPU. Single particle analysis was performed using CryoSPARC (Punjani et al., 2017).

### Crystallization and structure determination

The N-terminal acetylated and C-terminal biotin-pegylated 10-residue SARS-CoV-2 S2 peptide FKEELDKYFK (GenScript) was dissolved in 100% DMSO at 10 mg/mL and then diluted with PBS to 1 mg/mL. Fab WS6 was incubated with the peptide in a 1:2 molar ratio for 5 min to form complex. The Fab-peptide complex was concentrated to 10–15 mg/mL and screened for crystallization using 576 conditions from Hampton screen, Precipitant Synergy screen, and QIAGEN Wizard screen with a Mosquito robot mixing 100 nL reservoir solution and 100 nL protein solution per drop. Crystals were obtained from the solution containing 2% v/v PEG 400, 2 M  $(\text{NH}_4)_2\text{SO}_4$ , 100 mM sodium acetate, pH 5.5. Diffraction quality crystal were obtained by mixing 0.5  $\mu\text{L}$  WS6-peptide complex and 0.5  $\mu\text{L}$  of 80–100% concentration of the aforementioned crystallization solution. Crystals were cryoprotected with 15% v/v (2R,3R)-2,3-Butanediol in the aforementioned solution supplemented with 50% additional precipitant and flash frozen in liquid nitrogen for data collection.

X-ray diffraction data were collected at the Advanced Photon Source (beamline SER-CAT ID22). The diffraction data were indexed, integrated, and scaled with the HKL2000 package (Otwinowski and Minor, 1997). The structures were determined by molecular replacement with Phaser (McCoy et al., 2007) in the CCP4 Program Suite (Collaborative Computational Project, 1994). Further refinement was carried out with PHENIX (Adams et al., 2010), starting with torsion-angle simulated annealing with slow cooling. Iterative manual model building was carried out with COOT (Emsley and Cowtan, 2004) with maps generated from combinations of standard positional, individual B-factor and TLS refinement algorithms. X-ray data and refinement statistics are summarized in Table 1.

### Antibody germline assignment

Germline gene of heavy and light chain were assigned by querying nucleotide sequences on IGBLAST server. B6 heavy and light chain germline gene were assigned by submitting protein sequence. The V gene identity was reported as the identity to the germline nucleotide sequences.

### Antibody frequency calculation

The mouse Ig deep sequencing samples were prepared and used to predict probability of generation of specific protein sequences on CDR3. Human Ig deep sequencing samples were downloaded from Bioproject PRJNA511481. The Ig sequences were sieved for IGHV3 sequences (Sethna et al., 2019). The inferred models were used by OLGA to predict probability of having specific CDR3 sequences (Sethna et al., 2019). Signature of CV3-25 class antibody was defined as heavy chain IGHV5-51 and light chain IGKV1-12 germline gene, the R94, 96PQYC, G100b, C100d, and W100g on 18 amino acids CDR H3. The frequency of S2P6 class antibody was calculated by defining signature as IGHV1-46 germline gene with 97PKG in 11 amino acids CDR H3, and IGKV3-20 with Y91, 93SSPP and 96F on 11 amino acids CDR L3. The frequency of cc40.8 class antibody was calculated by masking IGHV3-23 with 94ITMA, 101V and 102V on 8 amino acids CDR H3 and IGLV3-10 with T91, 94SGN, and A96 on 11 amino acids CDR L3. The frequency of WS6 class antibody calculated by using mouse IGHV1-5 gene with 95TGS on 7 amino acids CDR H3, and IGKV4-61

gene with 91Y, 94Y and 96P on 9 amino acids CDR L3. B6 and IgG22 used identical heavy chain germline gene, although the light chain used different germline genes, it shared similar contact residues. B6/IgG22 class frequency was calculated by IGHV1-19 germline gene with CX{5,10}RX{4,6}W signature on CDR H3 amino acids, and IGKV8-27/IGKV1-99 germline genes with 92[LN] and 95[FY] on 8 amino acids length CDR L3.

### Phylogenetic analysis

Alpha-coronavirus spike sequences were downloaded using accession codes (NL63:Q6Q1S2.1, 229E:AOG74783.1, Feline:AA32596.1, Mink:ADI80513.1). Beta-coronavirus spike sequences were downloaded from NCBI server using accession codes listed in Full-length spike constructs. ClustalW was used to calculate neighbor joining (NJ) tree ([Larkin et al., 2007](#)), and Dendroscope was used to plot the Neighbor Joining tree ([Albrecht et al., 2012](#)).

### QUANTIFICATION AND STATISTICAL ANALYSIS

SPR sensorgrams were analyzed using Biacore S200 evaluation software using a 1:1 Langmuir binding model and plotted using GraphPad Prism. Crystal diffraction data and structural refinement statistics were analyzed with HKL2000, Phenix, and Molprobit ([Williams et al., 2018](#)). Statistical details of experiments are described in [Method details](#) or figure legends.